Biol Cybern
DOI 10.1007/s00422-011-0417-y

ORIGINAL PAPER

Biological Cybernetics

A simple model can unify a broad range of phenomena in retinotectal map development

Hugh D. Simpson · Geoffrey J. Goodhill

Received: 31 March 2010 / Accepted: 24 November 2010

Abstract A paradigm model system for studying the development of patterned connections in the nervous system is the topographic map formed by retinal axons in the optic tectum/superior colliculus. Starting in the 1970s, a series of computational models have been proposed to explain map development in both normal conditions, and perturbed conditions where the retina and/or tectum/superior colliculus are altered. This stands in contrast to more recent models that have often been simpler than older ones, and tend to address more limited data sets, but include more recent genetic manipulations. The original exploration of many of the early models was one-dimensional and limited by the computational resources of the time. This leaves open the ability of these early models to explain both map development in two dimensions, and the genetic manipulation data that have only appeared more recently. In this article, we show that a two-dimensional and updated version of the XBAM model (eXtended Branch Arrow Model), first proposed in 1982, reproduces a range of surgical map manipulations not yet demonstrated by more modern models. A systematic exploration of the parameter space of this model in two dimensions also reveals richer behavior than that apparent from the original one-dimensional versions. Furthermore, we show that including a specific type of axon–axon interaction can account for the map collapse recently observed when particular receptor levels are genetically manipulated in a subset of retinal ganglion cells. Together these results demonstrate that balancing multiple influences on map development seems to be necessary to explain many biological phenomena in retinotectal map formation, and suggest important constraints on the underlying biological variables.

Keywords Computational model · Topographic map · Visual map · Mathematical model · Axon guidance · Neural development · Retinocollicular

Electronic supplementary material The online version of this article (doi:10.1007/s00422-011-0417-y) contains supplementary material, which is available to authorized users.

H. D. Simpson · G. J. Goodhill (✉)
Queensland Brain Institute, The University of Queensland, Brisbane, QLD 4072, Australia
e-mail: g.goodhill@uq.edu.au

H. D. Simpson
e-mail: hugh.simpson@uqconnect.edu.au

G. J. Goodhill
School of Mathematics and Physics, The University of Queensland, Brisbane, QLD 4072, Australia

1 Introduction

A recurring feature of connection patterns in the brain is their organization into topographic maps (Udin and Fawcett 1988; Kaas 1997; Thivierge and Marcus 2007). A rich model system for understanding how such topographic maps develop is the formation of maps between the retina and the optic tectum (in fish, frogs, and chicks) or superior colliculus (SC, in mammals). Although the later refinement of such connection patterns is dependent on neural activity, their initial formation depends on molecular cues (Debski and Cline 2002; McLaughlin and O'Leary 2005). Sperry (1963) proposed that a key mechanism underlying the formation of maps by molecular cues is positional matching between input and target structures based on molecular gradients within these structures. Sperry observed that the level of molecular marker in a gradient can specify position, and hence also provide a means for map formation between regions with complementary molecular gradients. This is known as the chemoaffinity hypothesis (also, chemospecificity). Although

Published online: 22 February 2011

initial attempts to identify the molecular cues involved were unsuccessful, many constraints on the way such cues could operate were discovered by a combination of surgical manipulations of the retina and/or tectum, and theoretical modeling (Udin and Fawcett 1988; Goodhill and Richards 1999; Goodhill and Xu 2005). These studies suggested the involvement of mechanisms besides chemoaffinity, most notably competition between retinal axons for target space (Gaze and Keating 1972; Prestige and Willshaw 1975).

Subsequently, key molecules underlying chemoaffinity were identified to be members of the Eph receptor family and their ligands, the ephrins (Cheng et al. 1995; Drescher et al. 1995; Nakamoto et al. 1996; Pasquale 2005). Two distinct classes of Eph receptors, EphA and EphB, exist and interact with their corresponding ligands, ephrinA and ephrinB, respectively. Within each class there are a number of receptor and ligand subtypes, and the particular subtypes expressed typically vary between species. In general, the A-class interactions control the nasotemporal retina to rostrocaudal tectum/SC axis of the map, and the B-class interactions control the dorsoventral retina to mediolateral tectum/SC axis of the map (Fig. 1a).

These discoveries led to an accelerated recapitulation of the mechanistic arguments proposed earlier based on surgical manipulation studies. Initial suggestions that the maps form entirely by chemoaffinity-based mechanisms (e.g., Nakamoto et al. (1996); Honda (1998)) were rapidly modified as genetic manipulations of Eph and ephrin gradients revealed that chemoaffinity was insufficient by itself to explain the data (e.g., Feldheim et al. (2000)). Again competition was identified as a crucial constraint under many circumstances (e.g., Honda (2003)), though the generality of competitive mechanisms has recently been challenged (Gosse et al. 2008). The importance of receptor-based axon–axon interactions was highlighted by experiments on the effects of increasing the level of EphA in subsets of RGCs (Brown et al. 2000; Reber et al. 2004). These studies suggested that axon–axon interactions that depend on relative amounts of EphA between interacting axons exert important effects on topographic organization.

Few computational models have explored the mechanisms of these receptor-based axon–axon interactions. Furthermore, there has been little attempt to reconcile and integrate the findings of older surgical manipulation studies with more recent genetic manipulations. This leaves open the question of whether there is a coherent set of mechanisms which can naturally explain both the surgical and the genetic manipulation data. In this article, we show that this is indeed possible to do, using a relatively small number of assumptions, by updating an existing model of topographic map development. Starting with a framework originally developed in the Arrow model (Hope et al. 1976), Branch Arrow Model (Overton and Arbib 1982a), and eXtended Branch Arrow Model or XBAM (Overton and Arbib 1982b), we expanded the model to two dimensions and to include three competing constraints: chemoaffinity, competition, and a form of axon–axon interaction based on the evaluation of ratios of retinal receptor levels. We then submitted the model to a bank of experimental manipulations representing a cross section of surgical and genetic manipulations spanning several decades. We first show that the model is sufficient to reproduce a range of results, including: gross anatomical/surgical manipulations, the guidance of axons without competition (Gosse et al. 2008), and particular genetic manipulations (Brown et al. 2000; Reber et al. 2004). We then show that chemoaffinity and competition by themselves cannot reproduce the genetic manipulation results, and that receptor ratio-based axon–axon interactions are required. Unlike simple sorting models involving axon–axon interactions, our model explicitly considers both the initial ingrowth of branched retinal axons to the tectum/SC, and their subsequent trajectories across it. Together, our results reveal that a relatively simple mechanistic framework can explain a large and diverse range of data regarding retinotectal map formation.

2 Methods

2.1 Model description

The model we present in this article is based on the 2D Arrow model of Hope et al. (1976), the related 1D Branch Arrow Model of Overton and Arbib (1982a), and 1D eXtended Branch Arrow Model (XBAM) of Overton and Arbib (1982b). We consider a 2D mapping from RGCs in a square retinal array of unit side length to a continuous square tectum/SC, also of unit side length. Each RGC axon is assumed to end in an arbor containing several branches. The central equation of the model describes the movement of a branch b at each timestep in response to the "forces" of chemoaffinity, competition, and axon–axon interactions (Fig. 1b). This movement is given by the vector $\mathbf{M}_b$ as follows:

$$\mathbf{M}_b = m_1\mathbf{G}_b + m_2\mathbf{C}_b + m_3\mathbf{I}_b \tag{1}$$

The vector $\mathbf{G}_b$ in Eq. 1 represents a chemoaffinity-based axon **G**uidance mechanism, $\mathbf{C}_b$ describes a **C**ompetitive influence, and $\mathbf{I}_b$ represents axon–axon **I**nteractions. Each of these terms is weighted by a constant m_{1-3}. The axon–axon term, $\mathbf{I}_b$, is novel, and distinct from previous implementations of axon–axon interactions, in that the receptor ratio comparison is not relative to a particular tectal/SC axis (as in Hope et al. (1976); Overton and Arbib (1982a,b)), and includes an effect on growth cone motion (not modeled in Reber et al. (2004)). Defining the position of branch b as $\mathbf{x}_b$, at each timestep t this position is updated as:

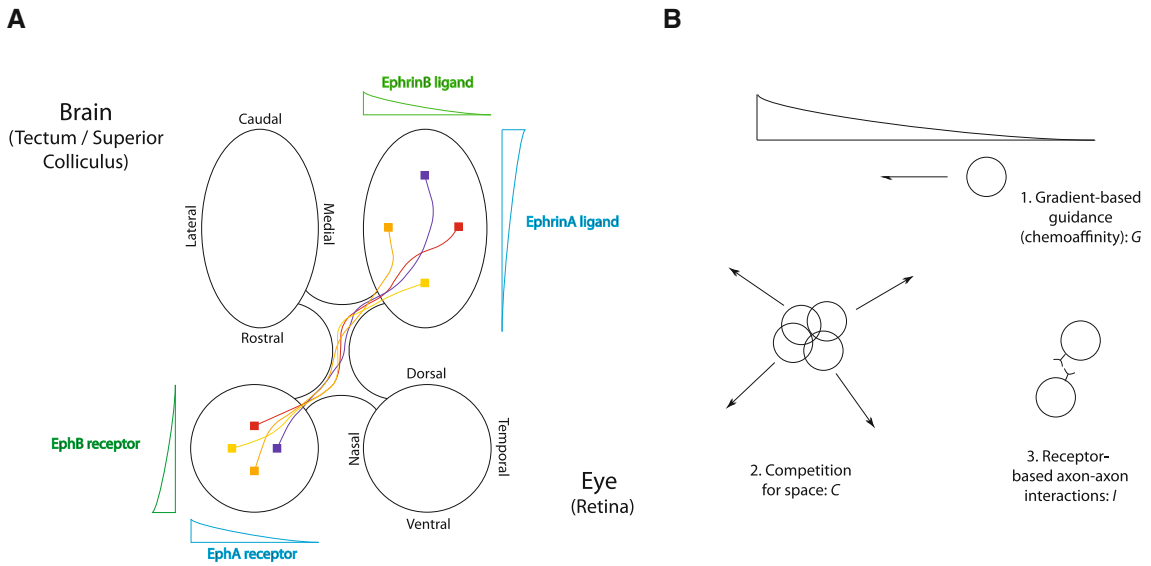

Fig. 1 Midbrain retinotopic maps and gradients. **a** Schematized version of the retinotectal/retinocollicular system, and the gradients of A and B-class Eph/ephrins that characterize them. The nasotemporal axis of the retina maps to the caudorostral tectum/SC, and is controlled largely by the A-class Eph receptors and ephrin ligands. High levels of EphA map to low levels of ephrinA, and low levels of EphA map to high levels of ephrinA (a repulsive interaction). The ventrodorsal retinal axis maps to the mediolateral axis of the tectum/SC, and is controlled largely by the B-class Eph receptors and ephrin ligands. In contrast to the EphA/ephrinA interaction, high levels of EphB map to high levels of ephrinB, and low levels of EphB map to low levels of ephrinB (an attractive interaction). There are subclasses of each type of receptor and ligand, whose presence and exact distribution vary between species; this diagram is a simplification of these situations but characterizes the general trends. **b** Schematic of mechanisms modeled. Axons experience a 'force' from each of: (*1*) guidance by chemoaffinity gradients; (*2*) competition for space; and (*3*) receptor-based axon–axon interactions (see Methods)

$$\mathbf{x}_{b,t+1} = \mathbf{x}_{b,t} + v\mathbf{M}_{b,t} \tag{2}$$

Here, v is a scaling parameter for the movement vector (or equivalently for the constants m_{1-3}); unless otherwise stated, it takes the value 1.

2.1.1 Chemoaffinity

Each branch is assumed to have a desired termination zone in the tectum/SC specified by molecular labels. The distribution of these labels is modeled implicitly; it is assumed that the mismatch between the present position and the desired position is proportional to the Euclidean distance between those positions, and that there is a tendency for each branch to move so as to reduce this mismatch. Axes are assumed to be independent. Writing the position of branch b's desired termination zone as $\mathbf{x}_{b_0}$, and the unit vector from $\mathbf{x}_b$ to $\mathbf{x}_{b_0}$ as $\mathbf{U}_G(b_0, b)$, the chemoaffinity term $\mathbf{G}_b$ for branch b is then:

$$\mathbf{G}_b = |\mathbf{x}_{b_0} - \mathbf{x}_b|\mathbf{U}_G(b_0, b) \tag{3}$$

$$= \mathbf{x}_{b_0} - \mathbf{x}_b \tag{4}$$

It is assumed that this chemoaffinity term can only operate while branches are on the tectum/SC.

2.1.2 Competition

The competition term $\mathbf{C}_b$ examines the proximity of other nearby branches (from the same or different axons), and models a competition for physical space in the tectum/SC. Effectively, it acts to move branch b to areas where there are fewer branches per unit area. The *branch interaction radius* r defines a small circle around each branch tip such that the branch tip may interact with any other branch tip that falls within this circle. Denoting the set of all other branch tips within this circle at a particular time as B_b, we can then write $\mathbf{C}_b$ as a sum of vector contributions from all branches k in B_b. Writing $\mathbf{U}_C(b, k)$ for the unit vector from branch b to branch k, the competition term is defined as a weighted sum of unit vectors:

$$\mathbf{C}_b = \frac{1}{|B_b|} \sum_{k \in B_b} W_d(b, k)\mathbf{U}_C(b, k). \tag{5}$$

The term $\frac{1}{|B_b|}$ ensures the sum is normalized, while $W_d(b, k)$ is a weighting with distance between branches, defined as:

$$W_d(b, k) = \begin{cases} 1 - \dfrac{d(b, k)}{2r} & \text{if: } d(b, k) \leq 2r \\ 0 & \text{otherwise} \end{cases} \tag{6}$$

where $d(b, k)$ is the Euclidean distance between the tip of branch b and the tip of branch k. Hence this term is maximal (with a value of one) if the branch fibers are at exactly the same position, and falls to zero when they are separated by a distance $2r$ (i.e., when the fibers cease to physically interact).

2.1.3 Axon–axon interactions

The axon–axon interaction term describes a tendency for nearby axons to be pushed apart if they have very different molecular labels, i.e., levels of EphA receptor. This is inspired by data describing fasciculation/defasciculation effects (Hayes and Meyer 1988; Bastmeyer et al. 1995; Caras 1997) and studies of the interaction of individual axons (Bonhoeffer and Huf 1985), and is related to the idea that axons cannot distinguish between themselves if they have similar levels of EphA (Brown et al. 2000; Reber et al. 2004). Denoting the receptor level of a branch as R, and using the mRNA EphA gradient profiles published in Reber et al. (2004), the EphA gradient along the retinal x (nasotemporal) axis is $R(x) = 0.26e^{2.3x} + 1.05$, where $x = (0, 1)$. We introduce a 'discrimination limit' parameter s, which is analogous to the discrimination limit discussed in previous experimental work on relative signaling (Brown et al. 2000; Reber et al. 2004); i.e., a critical value of EphA receptor ratios below which two interacting axons are indistinguishable. The interaction term for a branch b is then defined:

$$\mathbf{I}_b = \frac{1}{|B_b|} \sum_{k \in B_b} W_d(b, k)\mathbf{U}_I(b, k) \quad \text{if } Q(R_b, R_k) > s \qquad (7)$$

where $\mathbf{U}_I(b, k)$, $W_d(b, k)$, and B_b are as previously defined for the competition influence, and $Q(R_b, R_k)$ is a function that calculates the receptor ratios (and varies depending on the specific algorithm used, as described below).

If the calculated ratio $Q(R_b, R_k)$ is less than s (subthreshold), then the axons cannot discriminate between themselves and no interaction occurs. If, however, this value is above threshold, then a repulsive interaction occurs. We consider three algorithms corresponding to three choices for $Q(R_b, R_k)$ (see Table 1). The first condition $Q(R_b, R_k) = R_b/R_k$ describes the situation in which a branch b encounters another branch k where the receptor ratio is suprathreshold, and the branch with the higher level of receptor (b) is repelled. The second condition $Q(R_b, R_k) = R_k/R_b$ describes the case where similarly a suprathreshold interaction occurs, but instead the branch with the low EphA level is repelled. The third condition asserts that whenever there is a suprathreshold interaction, both axons are repelled. These conditions can be summarized respectively as: the growth cone with higher EphA is repelled, or the growth cone with the lower level of EphA is repelled, or both are repelled. We refer to these conditions in our model as forward, reverse, and bidirectional signaling, respectively.

Table 1 Axon–axon algorithms used in simulations

Algorithm	Condition
Forward signaling	$Q(R_b, R_k) = R_b/R_k$
Reverse signaling	$Q(R_b, R_k) = R_k/R_b$
Bidirectional signaling	$Q(R_b, R_k) = max(R_b/R_k, R_k/R_b)$

Three different variations of the axon–axon algorithm were tested and their effects explored. Unless otherwise stated, only forward signaling is used in figures presented here. (See Methods and Supplementary Information)

To understand how these mechanisms in our model relate to the biological concepts, first consider a gradient of EphA, $f(x)$, and a gradient of ephrinA, $g(x)$. If it is assumed that these gradients are multiplicative inverses, such that $f(x) = 1/g(x)$, and that their interaction obeys first order mass action kinetics (i.e., for a receptor R and a ligand L, the signal S generated by their interaction can be modeled as $S = RL$), then both forward and reverse signaling as referred to in our model have the same meaning as they do in purely biological contexts. That is, forward signal transduction occurs through receptors, and reverse signal transduction occurs through ligands (see Discussion for further details and Pasquale (2005) for more detailed descriptions of these concepts). Unless otherwise stated, all results use forward signaling (see Supplementary Fig. 6 for comparisons of these differing algorithms). Note, however, that the model presented here only uses receptor ratio comparisons in simulations, and hence does not rely on the stronger multiplicative inverse assumption—this assumption is only considered for interpretation and discussion of results.

There are currently no data supporting a similar discrimination limit for ephrinB/EphB interactions. In view of this, and the observations that these B-class interactions are typically attractive/adhesive rather than repulsive, we implemented repulsive axon–axon interactions for ephrinA–EphA interactions only. Note also that in the model, we have considered EphA, ephrinA, EphB, and ephrinB as single entities, whereas in reality these are classes of receptors and ligands, and there are multiple subtypes within each class. Individual receptor expression varies between species, but as both A and B-class receptors and ligands are represented in most species, and because functions within each class tend to be very similar, gradients are considered with these umbrella terms in the model. There are also other guidance molecules and neurotrophins which may play a role in retinotectal/retinocollicular map development, however, for simplicity we do not consider these. For a detailed summary of gradients involved in retinotectal/retinocollicular mapping see McLaughlin and O'Leary (2005); Scicolone et al. (2009).

2.1.4 Effect of tectal/SC borders

The above mechanisms are only applied to fibers on the tectum/SC. Experimental evidence suggests that axons grow toward the tectum/SC, even when initialized in ectopic locations (e.g., Harris (1982)). To account for this behavior, for fibers outside the tectum/SC a non-specific tendency to move toward the tectum/SC was included. Specifically, all fibers outside the tectum/SC experience a vector push perpendicular to, and in the direction of, the boundary of the tectum/SC. This applies both when axons are initially moving toward the tectum, and if they then move off the tectum after having arrived. This force is scaled down for fibers that are already on the tectum/SC, but are within r (the branch interaction radius) of a boundary. These fibers experience a push away from the boundary in addition to the movement vector $\mathbf{M}$ above. For a distance d from a boundary, the magnitude of this push scales as $1 - d/r$, and with direction perpendicular to the boundary (see Table 2).

2.1.5 Other differences with XBAM

The original XBAM included a 'Boundary' term which modeled interactions between fibers and graft boundaries/tectal borders, and an 'Averaging' term which gave fibers from the same axon the ability to influence each other. The latter term has been omitted, while the former has been replaced with the tendency (described above) for axons to move onto the tectum/SC if they are not on it, and away from a boundary. In addition, the fiber–fiber term has been split into separate competition and receptor–receptor interactions (Overton and Arbib (1982b) originally combined competition with 'switching' in the same term). In our simulations, the discarded mechanisms were either unnecessary and of no apparent influence, and/or were antagonistic toward other mechanisms. Further differences between the models are considered in the Discussion.

2.2 Simulations

Simulations involved a 20×20 grid of RGC axons, each with 8 branches, for a total of 3200 branches simulated. For all experiments presented, simulations with approximately $1000, 5000$, and 10000 branches were also run (Supplementary Fig. 4). Fibers were initialized in pseudorandom positions just outside the tectum/SC near the rostral border. At each timestep, influences were calculated to give the movement vector for each branch, and all branches moved simultaneously at each step. Results presented are after 1000 iterations, as running the simulations longer resulted in no significant change (data not shown; see also: Parameter Space Exploration below). Free parameter values are shown in Table 2. Sweeps of parameter space were performed in most experiments, and the ranges of values explored are quoted in Table 2 and in the relevant sections of the results. Unless otherwise stated, all results use a single parameter set (see below). Simulations were coded in Matlab and run on a local computing cluster. Pseudorandom numbers for initial positions were generated using the Matlab *randn* function.

Table 2 Table of parameters used in simulations

Parameter/variable	Value used	Range explored
Side of retina and tectum/SC	1	–
Iterations	1000	10^2–10^4
Axons	400	10^2–10^3
Branches per axon	8	1–12
Total branches simulated	3200	$\sim 10^3$–10^4
Branch interaction radius r	0.05	0.001–0.5
Relative signaling ratio s	1.1	0–10
m_1	0.02	0–2
m_2	0.2	0–2
m_3	0.15	0–2
Magnitude of border effect	0.1	0.01–0.5

Values represent those typically used in simulations. Where simulations used differing parameters, this is noted with the appropriate results. A range of values was explored in sweeps of parameter space. (See Methods, Results, and Supplementary Information)

In all results presented here, RGCs are initialized in a small rectangular zone just rostral to the tectal border: $x = (0, 1)$, $y = (-0.2, 0)$. Unless otherwise stated, fibers were distributed randomly within this zone. This was done by choosing an initial (putative) 'axon position' randomly, and then distributing branch fibers around this position in a normal distribution with a standard deviation (SD) of 0.1. In some animal species, there exists at least some degree of topographic ordering in the optic tract and nerve. We modeled this with a rough initial topographic bias in axonal position in both axes (within the rectangular zone rostral to the tectal border). This was done by choosing initial axonal positions from a normal distribution with SD $= 0.1$ around the topographically ideal position, and then again normally distributing branch fibers around these positions. Axons can be initialized at the rostral tectal border all at the same time, or ingrowth can proceed gradually, in a series of waves of ingrowth starting from more central retina and finishing with peripheral retina (Stuermer 1988; Stuermer and Raymond 1989; Pittman et al. 2008). For the waves of ingrowth simulations, waves occurred at iterations $1, 100, 200, 300, 400$ (final iteration remained 1000), and the sizes of the retinal arrays at these five points were $64, 144, 256, 324, 400$. Although all these possibilities for differing spatial and temporal ingrowth were explored, unless otherwise specified results use 'all at once' and unordered ingrowth. These ingrowth conditions are summarized in Table 3.

Table 3 Ingrowth conditions used in simulations

	Results presented	Values explored
Initial position	Rostral	Rostral or entire tectum/SC
Mediolateral ordering	None (random)	Rough or no (random) ordering
Rostrocaudal ordering	None (random)	Rough or no (random) ordering
Waves of ingrowth	All present at start	Progressive waves or all present at start

Conditions used in simulation results presented, and those explored in more extensive simulations (see Methods and Supplementary Information). Unless otherwise stated, all results used unordered ingrowth, with all axons present near the rostral tectal/SC border at the start of simulations

Table 4 Summary of EphA3 knock-in and EphA4 knock-out values used in simulations

	Chemoaffinity	Axon–axon
EphA3 $ki/+$	$ki_G = 0.25$	$ki_I = 1.6$
EphA3 ki/ki	$ki_G = 2$	$ki_I = 4$
EphA4 $+/-$	$ko_G = 0.125$	$ko_I = 0.7$

Values of EphA3 knock-in and EphA4 knock-out parameters used to model the experiments of Brown et al. (2000) and Reber et al. (2004). Knock-in and knock-out values were allowed to differ between chemoaffinity and axon–axon mechanisms

2.2.1 Modeling single axon topography

Analogous to the experiments of Gosse et al. (2008), we modeled retinotopic map formation when only single RGC axons were present. This was done by running 400 simulations which used only a single RGC—having 8 branches, for a total of 3200 branches simulated—and collating the data to obtain outputs of topography. These results were compared with one simulation which had 400 axons and hence 3200 branches, thus comparing 'sparse' (without other axons and hence without significant competition) with 'dense' (with other axons and with high levels of competition) while keeping the number of branches simulated consistent.

2.2.2 Modeling EphA3 and EphA4 manipulations

The EphA manipulations performed experimentally in mice (Brown et al. 2000; Reber et al. 2004) were modeled in the following manner. As per Reber et al. (2004), gradients of EphA of the form $R(x) = 0.26e^{2.3x} + 1.05$ were considered. A fixed knock-in amount ki was added to the receptor level $R(x)$ at alternate retinal positions to represent the EphA3 knock-ins, and in the case of the EphA4 knock-outs, an amount ko was subtracted from all retinal positions.

For the chemoaffinity mechanism, we calculated an effective shift in the desired positions of axons by taking the wild-type EphA gradient profile, and simply reading off the retinal position x' corresponding to the genetically modified receptor amount $R(x) + ki$ or $R(x) + ki - ko$ (Supplementary Fig. 1). Mathematically, this amounted to inverting the gradient function to find

$$x'(R) : x' = x'(R(x) + ki - ko) = \frac{\ln|(R(x) - 1.05 + ki - ko)/0.26|}{2.3}.$$

This allowed us to match the effect of the EphA manipulation to the wild-type map, without requiring details of other retinal and tectal/SC gradients.

The knock-in for the axon–axon interaction mechanism was simpler in that then receptor ratio comparisons were made directly between receptor levels. Competition did not involve EphA/ephrinA calculations, and hence the competitive component was unchanged from that described above. Because the chemoaffinity and axon–axon interaction mechanisms used the knock-in differently, we allowed the specific knock-in amount to differ between them. Unless otherwise stated, the heterozygote EphA3 knock-in for chemoaffinity, ki_G, was 0.25; and the heterozygote EphA3 knock-in for axon–axon interactions, ki_I, was 1.6. For the homozygote EphA3 knock-in, ki_G was set to 2 and ki_I to 4. Heterozygote EphA4 knock-outs were performed similarly, and took on values $ko_G = 0.125$ and $ko_I = 0.7$. These conditions are summarized in Table 4.

2.2.3 Parameter space exploration and sensitivity analysis

We systematically explored the parameter space of the model, testing a wide range of values constrained to be within biologically realistic ranges and assessing maps qualitatively. Fixed parameters (those with known or approximately known values, or values that could be estimated) were able to be restricted to smaller ranges and just a few values, whereas the free parameters (m_{1-3}) required a more thorough sweep through parameter space. These parameters were constrained to be positive, with a maximum value of 2; this upper bound was set because at each step this would allow a maximum step size for a particular influence to be equal to twice the tectal/SC side length. The following 10 values were considered for each of m_1, m_2, and m_3 in coarse initial sweeps of all experiments simulated: 0, 0.01, 0.1, 0.3, 0.5, 0.7, 0.9, 1, 1.5, 2. Hence 10^3 combinations of free parameter values were considered in each experiment; however, up to 10–20 values were used in finer sweeps for some experiments. Individual simulations generally took up to 1 h to run on single-core processor computers, while

sweeps through parameter space were performed on a multinode computing cluster.

Fixed parameters included the branch interaction radius r, and relative signaling ratio s, as these were readily identifiable with biological correlates which have values that could be estimated. The model's sensitivity to parameter values was analyzed by systematically varying their values about estimates/approximately known values. Actual ranges/values are shown in Table 2. The branch interaction radius r can be identified with the radius of a circular region that a growth cone might reasonably be able to explore with its filopodia during a given timestep. At minimum this should be the size of a growth cone, which when expressed as a fraction of tectum/SC size varies between species from approximately 0.001–0.05. (For example, a typical 10μm growth cone on a 1 cm chick SC gives the lower value, while the same growth cone on the approximately 200μm tectum of fish and frogs gives the upper value). This was limited to a maximum of 0.5 in simulations. A value for s has been approximated from experiments as 1.36 (Reber et al. 2004). We started with this value, and explored values from 0 to 10. In the EphA3 knock-in simulations, knock-in amounts were systematically varied along with discrimination limit, and axon–axon algorithm used. We also analyzed the step size scaling parameter, or growth cone velocity, v. This parameter v was varied from 0.01 to 5, but was set to 1 unless otherwise stated.

To ensure that the behavior of our model was stable in time, simulations were extended to 2500 and 10000 iterations and the resulting maps assessed. While they continued to refine, there was no qualitative change in map structures at these long times.

2.3 Trajectories and map precision

Axon trajectories were computed by taking the branch centroid, or 'center of mass' of the branch positions for each axon, and tracing this throughout simulations. Arbors were represented by connecting individual branch positions to the centroid.

Quantification of topographic maps generated by the model was complicated by the differing experimental manipulations modeled. We used a measure of distance to an 'ideal position' for each experiment, and this ideal position was calculated individually for each manipulation. For normal development, the ideal positions were simply a square grid of positions in the tectum/SC reflecting the square grid of retinal positions of origin of RGCs (with appropriate anatomical orientations). For the graft rotations and translocations, the ideal positions were similarly rotated and translocated. For expansion and compression simulations, the ideal positions were expanded and compressed relative to normal development, and so on. The actual measure calculated was averaged over individual fibers, so that the normalized distance D to the ideal position is calculated $D = (\mathbf{x}_{\text{ideal}} - \mathbf{x}_{\text{current}})/N_{\text{fibers}}$.

3 Results

We updated the Arrow (Hope et al. 1976) and XBAM (Overton and Arbib 1982b) models of retinotectal map formation, basing our version on the interaction of three constraints: chemoaffinity, competition, and axon–axon interactions. Growth cones are assumed to move in response to a vector sum of "forces" representing the influence of these constraints at each position in the tectum/SC (see Methods). Retinal axons are branched, but for simplicity we do not model the influence of molecular cues on branching; instead the focus is on the process of initial growth cone targeting to appropriate locations. We also do not model subsequent activity-dependent refinement of the mapping. Although it would be possible to include such effects, doing so is not required to address the range of phenomena we consider. It would also introduce many more parameters into the model, the values of most of which are hard to directly constrain from experimental data.

3.1 Normal development

For simplicity, many previous models of retinotectal map development have assumed that map development begins with all axons already on the tectum in a random or near-random order (Prestige and Willshaw 1975; Hope et al. 1976; Weber et al. 1997; Tsigankov and Koulakov 2006). However, in normal development in vivo, retinal ganglion cell (RGC) axons typically invade the optic tectum/SC rostrally or rostrolaterally (Harris et al. 1987; Gaze and Grant 1978; Kaethner and Stuermer 1992; Simon and O'Leary 1992), converging on their target from one direction. We therefore modeled RGC axons growing onto the tectum from a rostral location, either all together, or as a series of waves of ingrowth with central earlier-born RGC axons leaving the eye and reaching the tectum first before more peripheral later-born axons (e.g., Straznicky and Gaze (1971); Simon and O'Leary (1992); Pittman et al. (2008)). In both cases, a similarly ordered topographic map was formed (though slightly slower in the waves of ingrowth condition), with only trajectory shape varying between the two conditions (Fig 2a–e, see also Supplementary Movies M1, M2). When ingrowth proceeded in waves, axons experienced deviations from their trajectories due to the presence of axons already on the tectum/SC and also due to new waves arriving. When all fibers grew into the tectum/SC at the same time, axons experienced fewer deviations, and traced out broadly smoother trajectories (effect not quantified). These results suggest an important role for

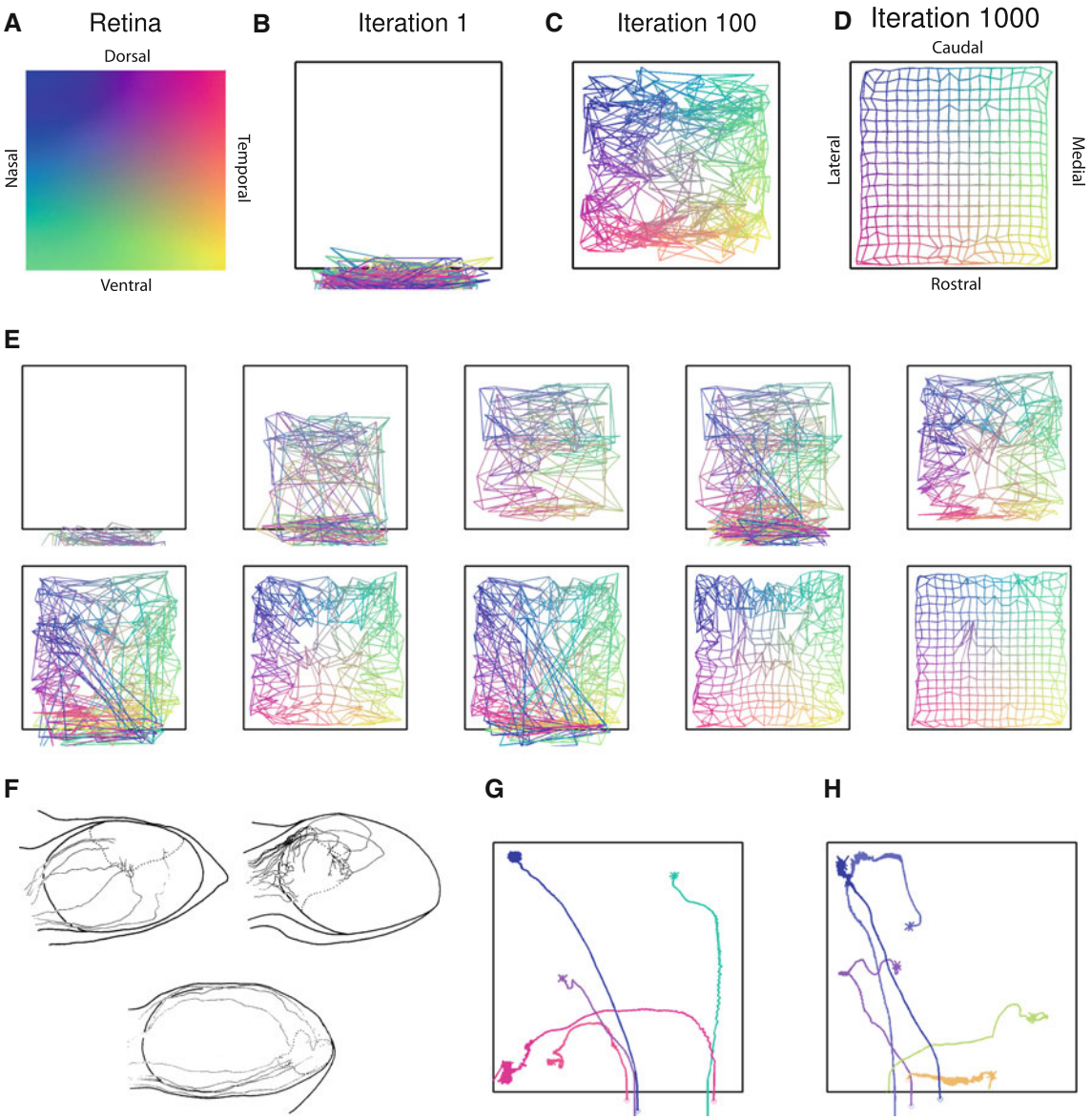

Fig. 2 Normal retinotectal map development. **a** Schematic of the retina, showing the color code used to label RGC axons in the tectum/SC in terms of where they originated in the retina. The nasotemporal axis of the retina maps to the rostrocaudal axis of the tectum/SC and the dorsoventral axis of the retina maps to the mediolateral axis of the tectum/SC. **b–d** Development of the map (at iteration 1, 100, and 1000, respectively) by axons growing from the rostral margin on to the tectum/SC, and then organizing into a map. In each panel individual RGC axons are represented by gridline intersection points, and axons originating from neighboring points in the retina are connected by gridlines (Supplementary Movie M1). **e** Ingrowth is now modeled as a series of waves from central to peripheral RGCs. Axons enter the tectum/SC in a stepwise fashion, mimicking the temporal order of arrival seen in vivo. Time progression is from left to right, and top row, then bottom row. **f** Sample trajectories from regenerating new taxons (rostral tectal border is to the left, reproduced with permission from Fujisawa (1981)). **g** Typical trajectories traced out by individual axons in the model for the conditions shown in (**b–d**). Model trajectories show similarities to the trajectories observed experimentally in **f** (Supplementary Movie M2). **h** Similar trajectory tracing, but now in the waves of ingrowth condition, as shown in **e**. There is now more variability in the trajectories of these early-born axons, due to the progressive discrete waves of ingrowth

competition in shaping trajectories, in addition to chemoaffinity.

We also tested the effect of increasing degrees of order within the optic nerve and/or tract, as is present in some animal models (Udin and Fawcett 1988). Some computational models depend on some initial bias within the optic nerve and/or tract to achieve smooth topography (e.g., Willshaw (2006)), whereas others require significant disorder within the initial map to achieve certain experimental results (e.g., Fraser and Perkel (1990)). Most models also do not test the

effect of the normal central-to-peripheral order of ingrowth. Hence it was important that the model presented here did not require any particular initial conditions, and further that its results were robust to changes in initial conditions. We found that this was the case, and in particular, that the model did not require any initial bias to generate topography (Supplementary Fig 2). The only noticeable differences in conditions of more or less order were changes in trajectory shape (Supplementary Fig 3). Hence, in addition to chemoaffinity and competition, initial position within the optic nerve/tract is important in shaping trajectories.

Examination of the trajectories of a typical subset of individual axons from such simulations shows that they are similar to those seen experimentally in some species (Fig. 2F–H, see also Supplementary Movie M2). Hence all other results presented here model all RGC axons growing in together, with no initial ordering within the optic nerve/tract.

3.2 Surgical graft experiments

A series of experiments in the 1970s and 1980s tested hypotheses regarding the mechanisms of retinotectal map formation by rotating and/or translocating pieces of retina and/or tectum (Udin and Fawcett 1988). These experiments showed that, if the manipulations were performed at an early enough developmental stage, the maps formed were consistent with the hypothesis that marker gradients were rotated/translocated together with the grafts (Yoon 1973; Hope et al. 1976). When a piece of tectum was rotated by 90° (Fig. 3a, Supplementary Movie 3) or 180 ° (Fig. 3b) in the model, it was found that the corresponding region of the resultant map was similarly rotated, consistent with these experimental data. Furthermore, when two pieces of tectum were removed and their positions exchanged without rotation (reciprocal translocation) in the model, again the resulting map followed the surgical rearrangement (Fig. 3c, Supplementary Movie 4). These results show that the model reproduces experiments that highlight the role of chemoaffinity in map formation. Such data have proved challenging to reproduce in some previous models (e.g., Hope et al. (1976)), and have not been addressed at all by others (Honda 2003; Yates et al. 2004; Tsigankov and Koulakov 2006).

3.3 Size disparity, mismatch, and compound eye experiments

Another type of surgical manipulation involves excising part of either the retina or the tectum to produce a size disparity between the two. In these cases, it was found that the retinotectal projection expands or contracts so as to smoothly map the whole of remaining retina to the whole of the remaining tectum (Yoon 1976; Schmidt et al. 1978; Udin and Fawcett 1988; Goodhill and Xu 2005). These experiments contradict the hypothesis that chemoaffinity labels rigidly specify the map, as well as computational models based on this assumption (e.g., Gierer (1987); Nakamoto et al. (1996); Honda (1998); Yates et al. (2004); Koulakov and Tsigankov (2004)). This conclusion was also reinforced by "mismatch" experiments, where, for instance, the nasal half of the retina and the caudal half of the tectum were both removed, leaving none of the normal correspondence between retinal and tectal labels. Despite this, a smooth map still formed (e.g., Horder (1971)). In a similar experiment, which preserves relative size between eye and brain but engineers a discrepancy between marker labels, compound eyes have been formed by joining two nasal half retinas together and allowing the projection to reform. Both halves expanded similarly to cover the whole tectal rostrocaudal extent, and remained topographic.

All these results can be reproduced using our model (Fig. 4, Supplementary Movies 5 and 6). In the retinal ablation and compound eye experiments, the influence of competition overrides the chemoaffinity influence, allowing expansion of RGC axons into normally inappropriate tectal territory. However an exception occurs if fiber density is low, in which case map expansion and mismatch performance are poor due to a lack of competition (see Supplementary Fig. 4). In the tectal ablation and mismatch experiments, the projections are compressed and shifted respectively, while maintaining topography, reflecting a balance in these simulations between competitive and chemical guidance influences.

3.4 Map ordering without competition

The importance of competition for retinotectal map formation has recently been questioned by the finding that individual RGC axons in zebrafish can still project relatively normally in the tectum even in the experimentally induced absence of other RGC axons (Gosse et al. 2008). We therefore modeled the ingrowth of only one RGC axon into the tectum (Fig. 5a). As expected, the axon terminated in its topographically correct location due to the chemoaffinity influence. This 'sparse' simulation was repeated for each of the 400 RGC retinal positions used in other results; the combined topography of these is shown in Fig. 5b. We then compared this with the topography in the normal or 'dense' case where all 400 axons grow in together (Fig. 5c,d). In this latter case, the effect of the competition term is to compress the termination zone of each axonal arbor. To quantify this effect, arbor sizes were calculated for each axon by taking the difference between most medial and most lateral fibers (x), and the difference between the most rostral and most caudal fibers (y). The resulting average arbor size in the dense simulation was $(x, y) = (0.041, 0.041)$, and for the sparse case $(x, y) = (0.23, 0.22)$; the distributions of arbor sizes had distinct means, with $P < 10^{-10}$ in a paired t-test. Thus, the

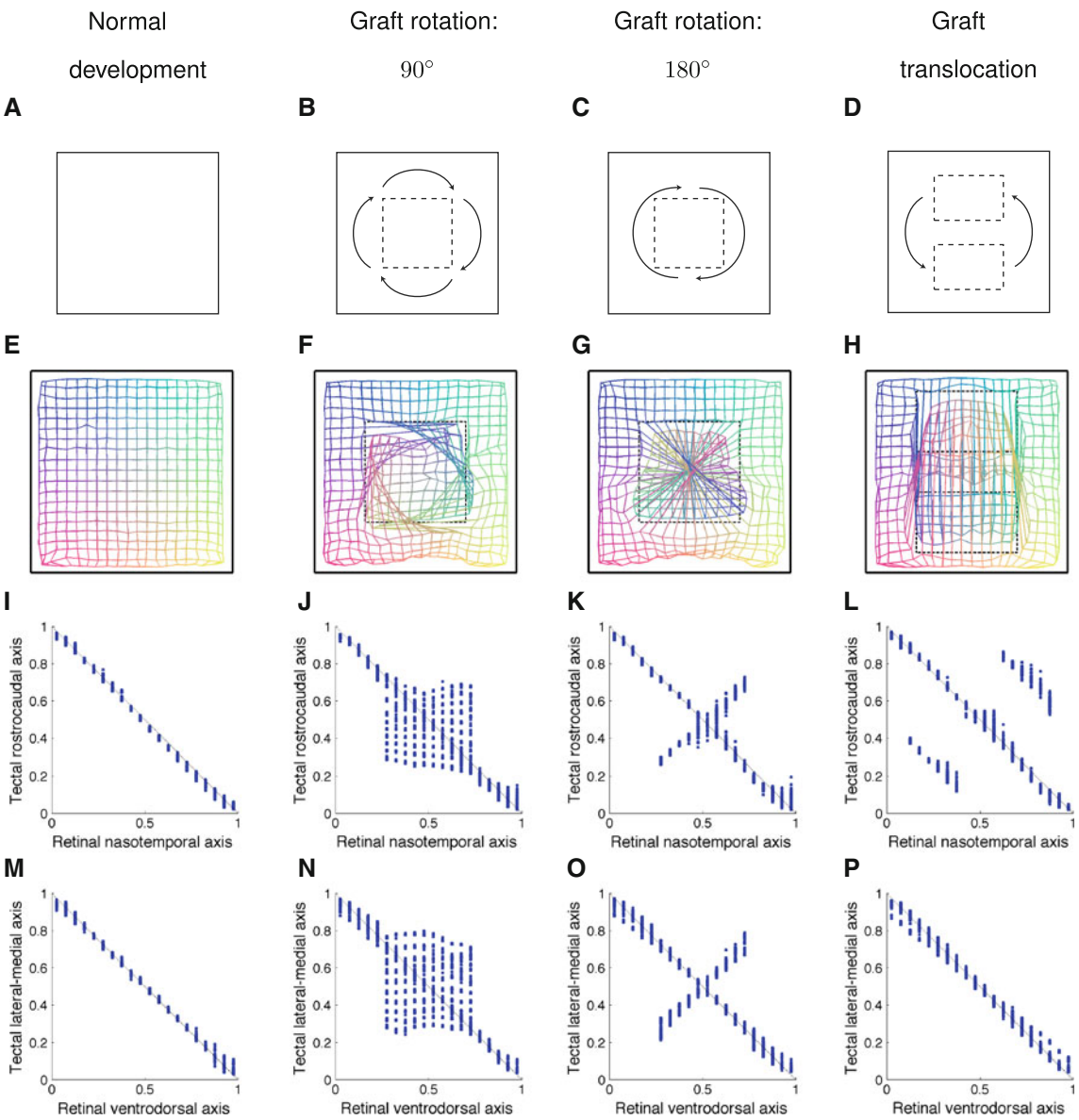

Fig. 3 Modeling graft rotations and translocations. Simulation results averaged over ten runs for graft manipulation experiments, and normal development for comparison (c.f. Fig. 1, in which only single simulation runs are presented). **a**, **e**, **i**, **m** Normal development. **b**, **f**, **j**, **n** 90° graft rotation. A central piece of tectum is excised, rotated 90°, replaced and allowed to re-establish connections (Supplementary Movie M3). **c**, **g**, **k**, **o** Similarly, 180° rotations are performed. **d**, **h**, **l**, **p** Now a translocation is made: two pieces of tectum are excised, have their positions exchanged, and are allowed to reconnect (Supplementary Movie M4). **a**–**d** Schematic representations of the experimental manipulations. **e**–**h** Corresponding model results in topographic grid form. Note in **g** that axons on the graft normally terminating in the bottom right of the target (colored *yellow*) now target upper left, as appropriate. Similarly, in **h** axons on a graft that normally target upper areas of the tectum (colored *blue-green*) now target lower. **i**–**p** Plots of single axis topography were created by plotting tectal positions against position of retinal origin for all branches in the simulations. **i**–**l** Single axis topography for the nasotemporal to rostrocaudal maps using branch positions. **m**–**p** Similarly, single axis topography for the dorsoventral to mediolateral map. For all three scenarios, the model matches the observed experimental behavior. Supplementary Movies 3 and 4 show stepwise evolution of a graft rotation and a graft translocation

model is consistent with the findings that competition is not required for a (mostly) normal map to form, but that when present it causes a compression of axonal arbors (Gosse et al. 2008). However, it is clear from Figures 3 and 4 that competition can play an important role in structuring perturbed mappings.

In the single axon simulations, fibers appear to be pushed away from their desired positions by competition until this force is balanced by chemoaffinity, while in dense simulations the same competition force is balanced out by the presence of many other fibers. In Fig. 5e, arbor size is plotted against branch interaction radius, and we see that there is

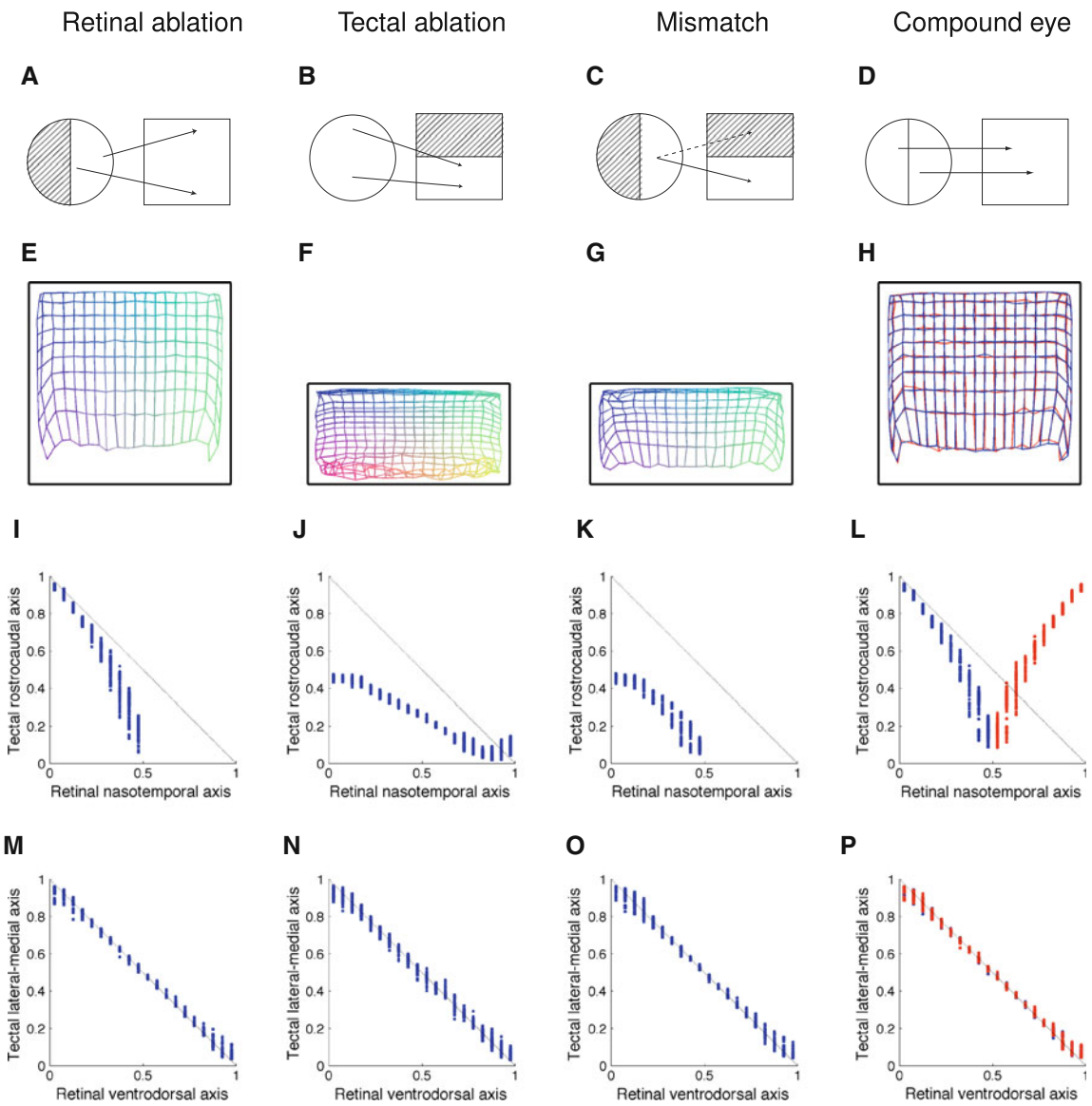

Fig. 4 Size disparity and mismatch experiments. **a**, **e**, **i**, **m** Retinal ablation (map expansion). When half of the retina is ablated the map expands to fill the entire tectum. **b**, **f**, **j**, **n** Tectal ablation (map compression). Similarly, when half of the tectum is ablated, and the map compresses to smoothly occupy the remaining tectal space. **c**, **g**, **k**, **o** Mismatch between retina and tectum. When half the retina and the non-corresponding half of the tectum are ablated, a smooth map is formed despite the mismatch of chemoaffinity labels. **d**, **h**, **l**, **p** Compound eye experiment, where two nasal half retinas are surgically fused. The two half retinas are shown in different colors; *blue* for the native half, and *red* for the half retina which has been surgically added. **a**–**d** Schematic representations of the experimental manipulations. **e**–**h** Grid representations of model results. **i**–**l** Single axis topography along the nasotemporal to rostrocaudal map matches that expected from these results: expansion, compression, and shift respectively. **m**–**p** Topography along the dorsoventral to mediolateral map is preserved in all simulations. In all cases, the map remains topographically ordered. Supplementary Movies 5 and 6 show stepwise evolution of retinal ablation and mismatch experiments

a strong correlation between the two quantities. In Fig. 5f, map precision (see Methods) is compared in the dense and sparse cases. Despite the increased arbor size in the sparse simulations, there is very little difference in the precision of the map between the two cases.

3.5 Collapse-like phenomena in simulations of EphA3 and EphA4 manipulations

A number of recent experiments have tested the contribution of ephrinA ligands and EphA receptors to map formation. In

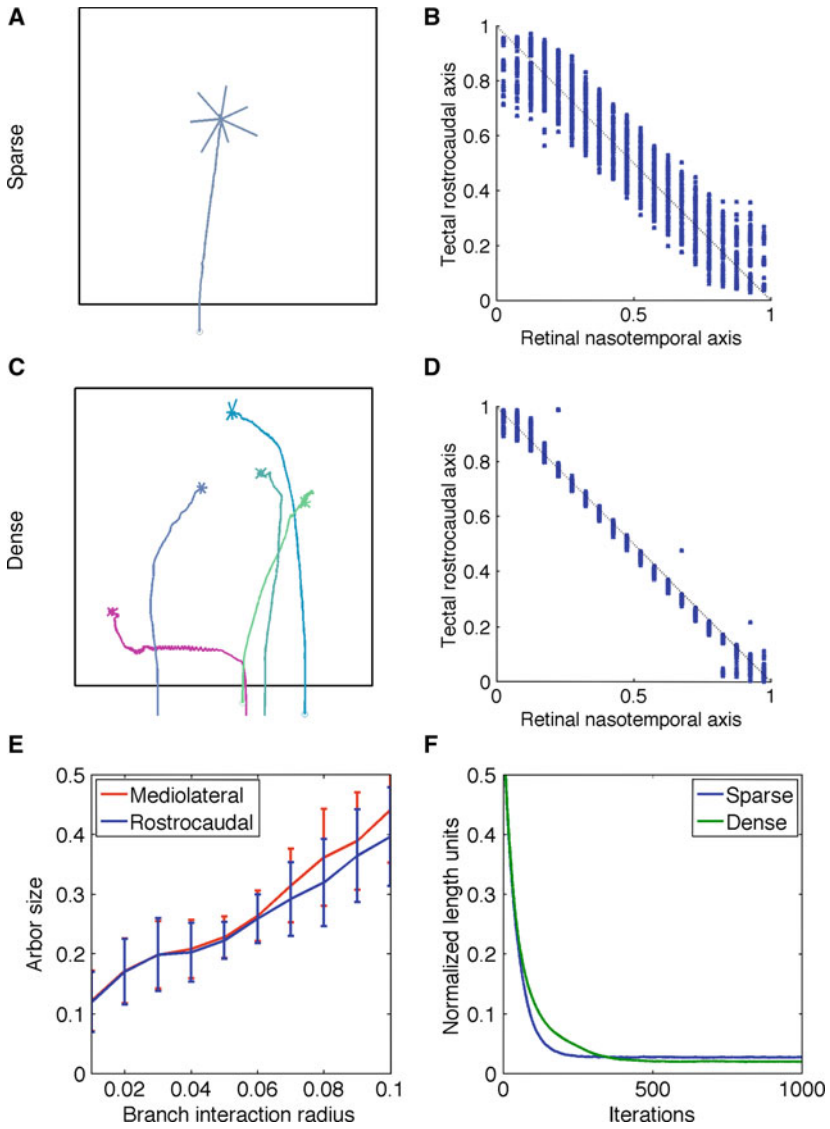

Fig. 5 Modeling the ingrowth of single RGC axons. 'Sparse' conditions (**a**, **b**) correspond to collated data from 400 simulations involving only one RGC, whereas 'dense' (**c**, **d**) refers to the normal RGC number conditions of one simulation with 400 RGCs. **a** Example of mature RGC arbor in the tectum in the single-axon simulations. **b** Topography along one axis (nasotemporal to rostrocaudal) of individual branch positions of RGCs obtained from 400 single-RGC simulations. **c** Mature arbors in the dense condition; five are shown here, with colors corresponding to position of retinal origin. **d** Single axis topography (nasotemporal to rostrocaudal) for the dense condition. Compression of arbor size is evident as expected in comparing **b** and **d**, similar to the experimentally observed compression (Gosse et al. 2008). **e** Arbor size (measured as rostrocaudal and mediolateral extent of the arbor, *blue* and *red* lines respectively) increases with branch interaction radius r. **f** Precision of the map, as measured using the proximity to ideal position value (see Methods), increases with time and is similar in both cases

the experiment of Brown et al. (2000), EphA3 was knocked-in to half of all RGCs (randomly distributed), while remaining normal in the other half. Experimentally, complete map duplication was observed in the homozygous case, with the knock-in map being spatially shifted relative to the wild-type map. However, in the heterozygous case, map duplication was observed only at one end of the SC (where EphA levels were the highest), while in the remainder of the SC the duplicated maps became indistinguishable (overlaid, rather than shifted); a phenomenon termed 'map collapse' by Brown et al. (2000). We modeled this EphA3 knock-in by adding a fixed amount to the EphA receptor level for alternate RGCs, and by specifying a corresponding shift in the normal termination site of each of their axons (see Methods). Our model was able to reproduce both map duplication and collapse results (Fig. 6). In these simulations, the wild-type and knock-in populations were separated across most of the SC, but were indistinguishable for the remainder.

To confirm this was a result of receptor ratio-based axon–axon interactions, and to examine the contributions of separate components of the model, the same simulations were run with either chemoaffinity only; chemoaffinity and competition; or chemoaffinity and axon–axon interactions. When only chemoaffinity was considered ($m_2 = m_3 = 0$), knock-in resulted in a second map being formed in addition to the normal map (Fig. 6d). These two maps result from the two sets of RGC axons mapping to their appropriate (but in the knock-in case, shifted) topographic location. However, the gap between the knock-in map and the wild-type map reduces as a function of the retinal axial position. This is due to the constant EphA knock-in value being proportionally less of the wild-type EphA value temporally c.f. nasally, as the wild-type EphA gradient is a positive exponential function of

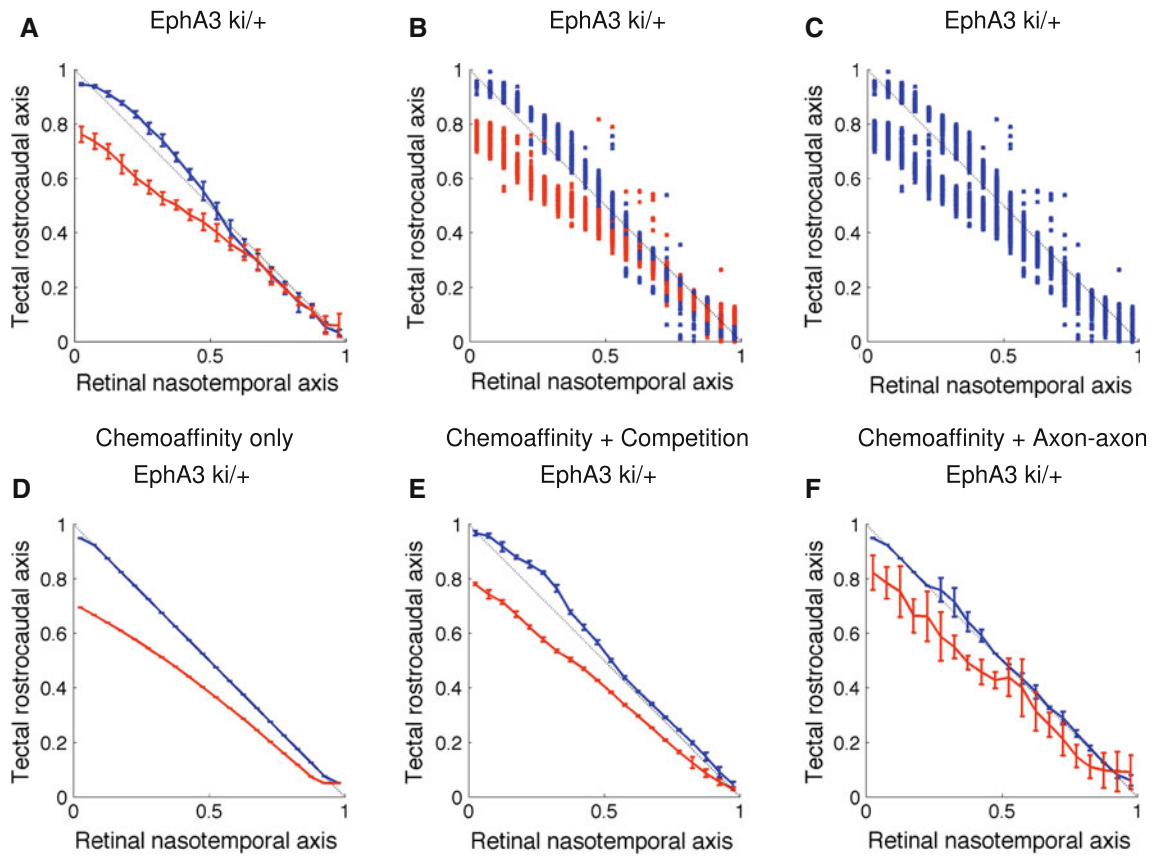

Fig. 6 Axon–axon interactions are sufficient to produce map collapse when receptor levels are varied in a subset of RGCs. The experiments of Brown et al. (2000) were modeled by adding extra EphA to 50% of RGCs (alternating). These populations are represented as *red* (knock-in) and *blue* (wild-type). Results presented are from a single run; averaged runs are presented in Fig. 7. Plots of single axis topography (nasotemporal to rostrocaudal map) are shown, using mean and standard deviation (SD) of axon position (**a**, **d**, **e**, **f**), or individual fiber positions (**b**,**c**). **a–c** A phenotype similar to the collapse of duplicated maps is observed, whereby the maps are duplicated in most of the SC but collapse to a single map in the remainder, as observed in heterozygote EphA3 knock-ins (Brown et al. 2000). Collapse is demonstrated in axonal positions (mean and SD shown) in **a**, and in individual fiber positions in **b**. Although using different colors for different populations is useful for visualizing the model, for better comparison with the experiment (where these wild-type and knock-in fibers are essentially indistinguishable) a single color plot is included (**c**). Note that the two populations intermingle at approximately 0.4 along the rostrocaudal tectal/SC axis (or approximately 0.6 along the retinal nasotemporal axis), comparable to the situation observed experimentally. To tease apart contributions from individual mechanisms to the collapse phenomenon, different combinations of mechanisms were modeled. **d** Chemoaffinity alone ($m_2 = m_3 = 0$). The knock-in causes the maps to separate, and this map separation reduces as a function of retinal axis position. **e** Chemoaffinity and competition ($m_3 = 0$). Maps remain separated, and competition causes slight shifts in map position from the chemoaffinity only case, but there is no collapse. Hence in the model, axon–axon interactions are necessary to cause map collapse. **f** Chemoaffinity and axon–axon interactions ($m_2 = 0$). Despite showing a trend towards map collapse, maps remain separated, suggesting that axon–axon interactions are not sufficient to cause complete map collapse. Hence map collapse in our model requires chemoaffinity, competition, and axon–axon interactions working together (**a–c**), and is thus dependent on the combined effect of all constraints

retinal axial position (Supplementary Fig. 1). Although the two maps move closer in this condition, they do not collapse. When competition was added ($m_3 = 0$) both the wild-type and knock-in maps were shifted (Fig. 6e). Although the gap between the maps remained similar to that in the chemoaffinity-only case, both maps were pushed slightly away from their chemoaffinity-only positions. Neither of these cases reproduced the experimentally observed collapse of the dual map to a single map observed experimentally, hence we can conclude that axon–axon interactions are necessary for map collapse. But are they sufficient? Fig. 6f shows a simulation with chemoaffinity and axon–axon interactions, without competition ($m_2 = 0$). Although maps trend towards each other more in this case, complete map collapse is not observed. This suggests that map collapse requires chemoaffinity, competition, and axon–axon interactions all acting together, and therefore that map collapse is a truly multiple constraint phenomenon. (See Methods for details of parameters used in these results, and Discussion for a comparison with experimental estimates of these parameters).

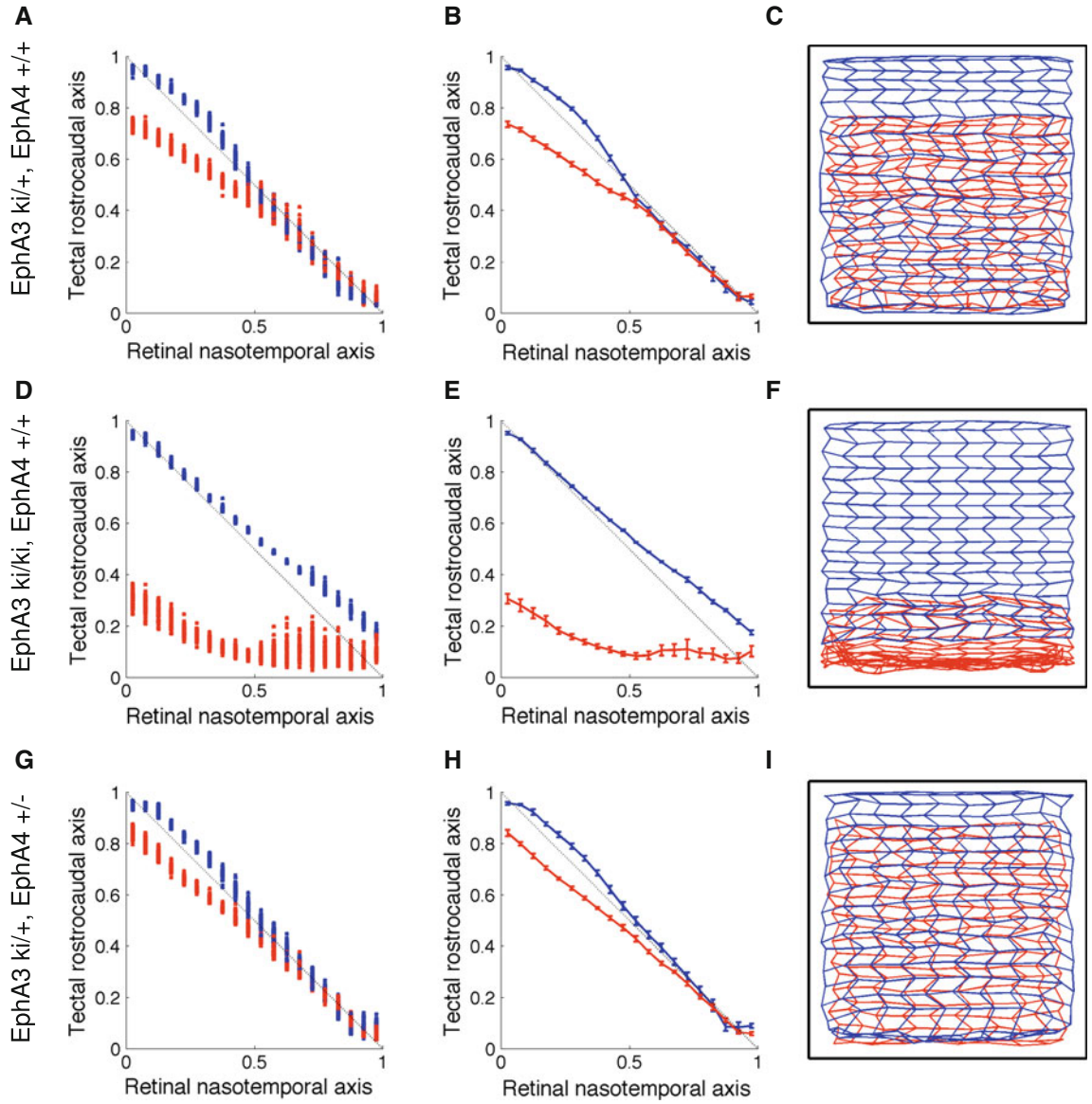

Fig. 7 Map duplication and collapse in EphA3 knock-in and EphA4 knock-out phenotypes. From *left* to *right* (all rows): individual fiber positions (*left column*), mean and standard deviation of axon positions (middle column), and modified topographic grids for each case. The modified grid now displays each population as a separate grid. In all figures, mutant (knock-in) RGCs are colored *red*, while wild-type RGCs are *blue*. Each row consists of plots of data obtained by averaging over 10 simulations. **a**, **b**, **c** EphA3 *ki*/+ EphA4 +/+ case, as in Fig. 6a–c, but now averaged. Doubled maps approximate or 'collapse' at approximately 55% of the nasotemporal axis, and grids transition from being separate (upper region of **c**) to being overlaid (lower region of **c**). **d**, **e**, **f** EphA3 *ki*/*ki* EphA4 +/+ case. Although significant shifts are still observed in the knock-in population and parts of the wild-type populations, the maps no longer collapse, and are separated in proportion to the increased amount of EphA3 knocked in. Note the topographic grids are now shifted in their entirety. **g**, **h**, **i** EphA3 *ki*/+ EphA4 +/− case. Here, the results of Reber et al. (2004) are modeled, where a heterozygote EphA4 knock-out in all RGCs is performed in addition to the heterozygote EphA3 knock-in alternate RGCs. The model again reproduces the experimentally observed map collapse, but in a smaller region than in the heterozygote EphA3 knock-in alone

We next explored the gene dose-related effects of EphA manipulation by modeling homozygote EphA3 knock-ins in a similar manner to that described for the heterozygote case above, and then extended the analysis to include a heterozygote EphA3 knock-in combined with a heterozygote EphA4 knock-out (based on the experiments of Reber et al. (2004); see Methods). In agreement with experimental observations, larger knock-ins resulted in complete separation of the two maps (Fig. 7d–f; Supplementary Fig. 5). Adding an EphA4 heterozygote knock-out maintained an area of map collapse, but the collapsed area was smaller, as observed experimentally (Fig. 7g–i). Together, these results suggest

that receptor ratio comparisons, as suggested by Brown et al. (2000); Reber et al. (2004), in concert with repulsive/competitive interactions between axons, can indeed result in a map collapse phenotype.

3.6 Surgical and genetic manipulation experiments can be reproduced from just one set of model parameters

The model presented here reproduces a broad range of experimental results using a single set of parameters (see Table 2). Thus, both surgical and genetic manipulation experiments from different species can be unified in one modeling framework with just one set of parameters. This particular set of parameters was chosen based on sweeps of parameter space for all simulations, and although a large subset of all possible parameters gave reasonable results for individual manipulations, fewer gave reasonable results for all (see Supplementary Material for detailed discussion of parameter sensitivity).

In Fig. 6, the special case $m_3 = 0$ was addressed to show that when axon–axon interactions were absent, map collapse did not occur in the model. For all other experiments considered here axon–axon interactions were in fact not necessary to obtain similar results. The results for $m_3 = 0$ for other experimental situations are included in Supplementary Fig. 7. The main differences between the maps generated with axon–axon interactions and those without are that the former are slightly less precise than the latter in certain surgical manipulations (only evident on quantification; Supplementary Fig. 8), and that axon trajectories have more deviations when axon–axon interactions are included (data not shown). This extra map noise has a consistent pattern, and is greater where absolute receptor levels are higher (generally rostrally; e.g., Fig. 4f, i). This appears to result from more frequent axon–axon interactions that are below the discrimination limit.

To better quantify the relationship between parameter values and map precision, model parameters were systematically varied and plotted in Fig. 8 against the 'distance to ideal position' measure of map precision (see Methods). For simplicity we held all parameters constant except the one in question. The branch interaction radius demonstrated optimal values from 0.02 to 0.06, consistent with approximate growth cone size of common model animals used in midbrain retinotopic map experiments. The lack of precision at lower values indicates that competition and axon–axon interactions (which depend more strongly on this value) lose effectiveness in this range. Higher values become biologically unrealistic and lead to excessive effects from competition and axon–axon interactions, and attenuated effects of chemoaffinity. The velocity scaling factor v shows optimal values around 1, consistent with the notion that low velocities take too long to form maps while higher velocities cause constant overshoot. The discrimination limit shows a different trend, with peak precision around 1. Given that neighboring axons should have ratios close to one, it is intuitive that values much higher than one cause the axon–axon interaction to have little or no effect. The coefficients for the three free parameters (controlling competition, axon–axon interaction, and chemoaffinity strengths) show similar trends in that lower values generally result in higher precision. This is likely to be due to higher values giving such large movement vectors that targets are overshot in one movement at each iteration, and as such the fiber position tends to oscillate around the ideal position (sometimes with large amplitudes).

4 Discussion

We have demonstrated that a relatively simple model of retinotectal/retinocollicular map formation based on the Arrow (Hope et al. 1976) and XBAM (Overton and Arbib 1982b) models can unify a wide range of apparently disparate experimental results from both surgical and genetic manipulations. Although a combination of chemoaffinity and competition are sufficient to account for some experimental findings, our results suggest that axon–axon interactions, in the form proposed by Reber et al. (2004), are required to cause the collapse of a doubled map to a single one when receptor levels are artificially increased. These areas of map collapse appear to be a result of axon–axon interactions creating areas of greater competition than in normal maps, with resultant shifts in parts of the axonal population. Together these results argue that the graded interaction of multiple constraints may be a principle underlying retinotectal/retinocollicular map formation across a wide variety of circumstances.

4.1 Mechanisms of the model

Employing a more abstract "implicit" chemoaffinity mechanism in the model is a simplification, but this allowed us to examine the effect of axon–axon interactions without the potentially confounding influence of particular choices of chemoaffinity mechanism. Choosing a specific mechanism would typically involve many more parameters, and necessitate some arbitrary assumptions, given that the biological data regarding chemoaffinity is unclear as to specific biophysical mechanisms. Leaving the chemoaffinity mechanism as abstract/generalized allows us to tease apart the mechanisms behind retinotectal mapping, without the above problems. Examining and comparing specific chemoaffinity mechanisms, such as the servomechanism model (Honda 1998), is beyond the scope of this article.

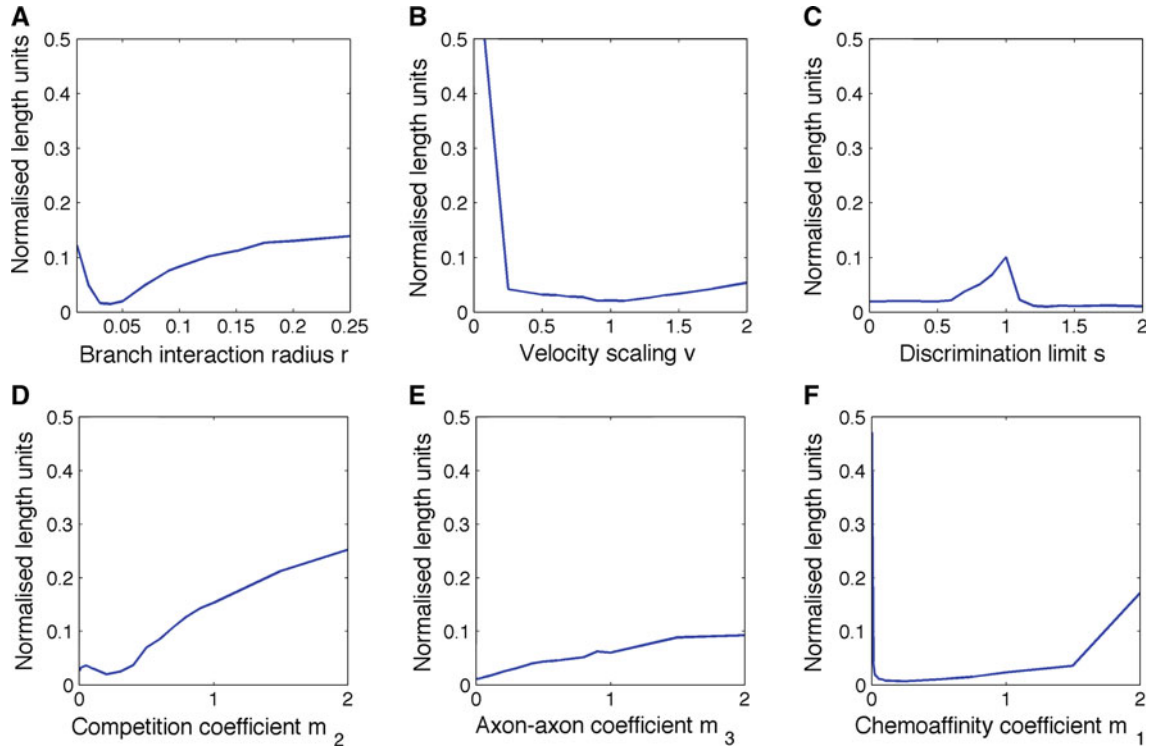

Fig. 8 Variation of map precision with system parameters. All panels: Map precision plotted against parameter values for the branch interaction radius r, velocity scaling constant v, discrimination limit s, and m_{1-3}. Map precision here is read out in terms of distance to ideal position, i.e., closeness to the ideal topographic map (see Methods). This measure uses normalized length units, as for other simulations, such that tectal/SC length and width vary between (0, 1). All plots are for normal development. **a** Values of the branch interaction radius r between 0.02 and 0.06 give the greatest precision. **b** Except at very low velocities, precision is relatively insensitive to varying the velocity of growth cones v. **c** Only values of the relative signaling threshold s close to unity affect precision significantly, and there is an asymmetry about 1. **d–f** Increasing the competition coefficient m_2, axon–axon interaction coefficient m_3, or chemoaffinity coefficient m_1, gradually decreases precision, but the magnitude of this effect varies between the three mechanisms

Competition in the model is represented using a distance dependent repulsion, because this models a competition for target space, and is advantageous in that it requires little parameterization (having only one fixed parameter, identifiable with growth cone size). Although mathematically similar, the mechanisms of competition and axon–axon interactions in our model are quite distinct. In the axon–axon interaction, the repulsion is experienced by only one out of the two interacting fibers and is thresholded, compared to the unthresholded bilateral repulsion of the competition term. Also, the different coefficients m_2 & m_3 allow the magnitude of these effects to vary. These mechanistic differences translate into different effects, as can be seen, for example, in Fig. 6.

Explicit gradients are employed for the axon–axon interaction because, in contrast to data for the chemoaffinity mechanisms, quantitative measurements of the relevant parameters are available (Reber et al. 2004). Assumptions regarding thresholded repulsive axon–axon interaction are based on the demonstration of this type of behavior for EphA–ephrinA interactions (Hansen et al. 2004; McLaughlin and O'Leary 2005; Pasquale 2005). We have not included EphB–ephrinB class axon–axon interactions in this model, given that there is not the same evidence for these interactions as there are for the A-class interaction (see Methods). B-class interactions are likely to be attractive/adhesive in nature and hence may modulate the repulsion effect of the EphA–ephrinA interaction.

4.1.1 Activity-dependent and activity-independent mechanisms

We do not include correlated neural activity in our model for two main reasons. First, it is generally accepted that an initial coarse map is set up by activity-independent cues, and that although this map is subsequently refined by neural activity, this activity is not essential for organizing global topography (Ruthazer and Cline 2004; McLaughlin and O'Leary 2005). Second, we have aimed to develop a model of map formation with as few assumptions and parameters as possible, and introducing activity brings many more of both of these.

4.2 Comparison with other models

Several previous theoretical models have made important contributions to our understanding of the mechanisms involved in retinotectal map development (reviewed in (Willshaw and Price 2003; Goodhill and Xu 2005; Simpson et al. 2009)). Surprisingly though, there have been few attempts to create a unifying model of map development that is capable of explaining normal and perturbed development using the one framework and parameter set. Godfrey et al. (2009) created a detailed model of retinocollicular map formation, but only considered the development of the normal map. Other models have tackled a broader data set, including the models of Willshaw and von der Malsburg (1979); Willshaw (2006) and Weber et al. (1997). These models have been submitted to a battery of experimental result comparisons, although of these only the model of Willshaw (2006) attempted to engage with more modern genetic experiments. In our results, we address a larger data set, including both surgical and genetic manipulations, and use only the well-established mechanisms of competition and chemoaffinity, along with axon–axon interactions based on recent experimental work.

Models based on rigid chemoaffinity constraints, while providing an account of normal development, are unable to explain the plasticity observed in perturbed situations (Gierer 1987; Honda 1998; Yates et al. 2004). Although modifications to some of these models allow for some plasticity (Gierer 1983; Honda 2003), they have still only been applied to a relatively limited range of data. The model of Gierer (1983) employs an indirect form of axon–axon interaction through its 'regulation' mechanism, which has similarities to the retinal induction mechanism proposed by Willshaw and von der Malsburg (1979). Our model differs from these since we use competition and receptor ratio-based axon–axon interactions independently, and both of these mechanisms are well-grounded in the experimental literature. Sorting models (Hope et al. 1976; Koulakov and Tsigankov 2004; Tsigankov and Koulakov 2006) assume that all axons are already present in the tectum/SC and consider only an abstract 'swapping' of the positions of terminal arbors. This fails to explain the smooth trajectories of axons growing into and rearranging within the tectum/SC that we have demonstrated in our model. These models are also unable to address the ingrowth of isolated axons as in the experiments of Gosse et al. (2008).

Most other models do not attempt to address both systems-level and genetic perturbations, and from their assumptions it seem unlikely that they would be capable of this without significant changes. Multiple constraint models have shown more success at reproducing systems-level perturbations (Overton and Arbib 1982b; Fraser and Perkel 1990), as have some models that considered how activity-dependent and molecular cues might interact to determine map structure under a variety of conditions (Whitelaw and Cowan 1981; Cowan and Friedman 1991; Weber et al. 1997). However, these models have generally not been updated to take account of data from genetic manipulation experiments. An exception to this is the marker induction model, which has not only demonstrated that it can replicate many of the surgical style manipulations presented here (Willshaw and von der Malsburg 1979), but it has also been recently modified and applied to EphA genetic manipulation experiments (Willshaw 2006). The marker induction model relies on the assumption that molecules on retinal axons directly modify the gradients present in the tectum/SC. Although direct evidence for this mechanism is limited, it has been shown to be effective in topographic organizing behavior in a range of scenarios.

4.2.1 Comparison with XBAM and Arrow models

The original XBAM (Overton and Arbib 1982b) considered the summed effect of vector influences on growth cone motion and was successfully able to reproduce a number of surgical manipulations in 1D. This success was in part why we updated and expanded the model to tackle larger datasets. While here we have addressed in 2D some of the same surgical manipulations that were modeled in 1D in the original XBAM, we have also included other surgical manipulations not modeled in the original (mismatch, 90° graft rotation) as well as the newer genetic manipulations, and conditions of reduced competition.

There are a number of advantages of this 2D model over the original 1D model. Some experiments simply cannot be modeled in 1D (such as 90° rotations), while others have altered and/or more complex geometry in 2D (180° rotation, translocation) so that results may be expected to differ in 1D versus 2D. Some mechanisms also have a different geometry and form in 2D (e.g., axon–axon interactions), and the effect of mechanisms differs when fibers can move in two dimensions. As a result, we can realistically trace trajectories in 2D, but not in 1D.

We note that although XBAM was in 1D, the model upon which XBAM was based, the Arrow model (Hope et al. 1976), was in 2D. This allowed the Arrow model to be applied to 90 ° rotations and translocations, but in contrast to our model, the Arrow model employed discrete arrays for the pre- and post-synaptic neurons, and used only one influence (a 'switching' algorithm).

4.2.2 Comparison with Reber et al. (2004)

The model presented here is consistent with the general assumptions and data presented in Brown et al. (2000); Reber et al. (2004), but is different from the quantitative

model presented by Reber et al. (2004) in several ways. First, the model we present uses a simple but biologically plausible implementation for how relative signaling is carried out, based on established EphA/ephrinA behavior. Second, an explicit and complete framework (using multiple constraints/influences) is presented, and simulations of map development under various conditions are carried out. Third, although we reach similar conclusions to those of Reber and colleagues regarding the importance of relative signaling, these ideas are developed further in our model by examining the mechanisms for how this might be implemented biologically, by showing how it relates to other mechanisms of map development, and by considering alternative interpretations of the relative signaling idea (see below).

We have shown that using multiple constraints, it is not necessary to assume that axons compare themselves with a 'dominant polar reference cell' to explain wild-type maps. Nor is it necessary to speculate on the involvement of additional mechanisms (such as correlated activity) in shaping the map in areas where the local relative signaling ratio falls below the discrimination limit. In contrast, in the model presented here, wild-type maps are largely governed by the well-established chemoaffinity hypothesis (Figs. 2, 3), while collapse behavior requires all three mechanisms acting together in a graded fashion (Fig. 6). Axons are guided weakly by chemoaffinity, duplicating the topographic map, but bringing the duplicated maps closer together rostrally, which aids in map collapse (Fig. 6d). The addition of a stronger competitive influence provides a generalized competition for target space, which can be modulated by the axon–axon interaction (Fig. 6e). Adding local interactions between axons using their EphA receptors creates regions of greater and lesser competition throughout the tectum/SC, breaking the duplicated maps' symmetry and allowing areas of collapse to form (Fig. 6a–c). Hence, we suggest that map collapse in EphA3 knock-in experiments is a truly multiple constraint phenomenon, for which each of the three constraints modeled are necessary, but none is sufficient alone.

To reproduce the EphA manipulation results, we did not attempt to exactly match the parameter values of our model to the values suggested in Reber et al. (2004). For instance, the parameter determining the effect of the knock-in on chemoaffinity was allowed to vary independently from the parameter determining the effect of the knock-in on axon–axon interactions (Table 4), since there is no reason to think these two quantities will scale in exactly the same way. In addition, the gradients measured by Reber et al. (2004) were mRNA rather than protein, and no error estimates were given for some of the numbers quoted (e.g., the signaling ratio of 1.36 and collapse point of 76%), or for the precise structure of the maps.

The algorithm for axon–axon interactions in our model offers an alternative interpretation for the relative signaling mechanism. We have assumed that two nearby growth cones can interact, compare EphA levels, and experience repulsion if this ratio is above a threshold. However, this 'receptor ratio comparison' seems like a difficult task for growth cones to perform. We can arrive at a simpler explanation if we assume that gradients in pairs such as ephrinA and EphA are at least approximately multiplicative inverses (e.g., e^x and e^{-x}), so that we can write the discrimination limit as a product of EphA and ephrinA levels, rather than a ratio of EphA receptor densities. This then resembles a typical mass action interaction between receptor and ligand, and both repulsive and thresholded characteristics of this interaction are supported in the literature (Wilkinson 2001; Hansen et al. 2004; Pasquale 2005). The multiplicative inverse gradient idea is lent support by the previous assertions by others that a servomechanism-type mass action law exists for the EphA–ephrinA interaction, and that this controls retinotectal/retinocollicular mapping (Nakamoto et al. 1996; Honda 1998; Hansen et al. 2004). Essentially, if one assumes a servomechanism rule with $S_0 = RL$ (where S_0 is a signal produced by the interaction of a receptor R and ligand L), then this implies gradients are multiplicative inverses within a factor of S_0. Similarly, a multiplicative inverse rule implies a servomechanism rule with $S_0 = 1$. Hence with only some simple and plausible assumptions, the EphA receptor ratio comparison with threshold—a rather abstract concept—can be reduced to a more familiar mass action rule, one for which thresholded/biphasic behavior has already been demonstrated.

4.3 Species differences

In chicks and mice, the predominant guidance mechanism for RGC axons in the tectum/SC appears to involve biased interstitial branching according to Eph/ephrin gradients, rather than the directed growth due to the same gradients as seen in lower vertebrates such as fish and frogs (McLaughlin and O'Leary 2005). We did not directly model interstitial branching, yet our model can produce a map collapse phenomenon similar to that observed in mice. This suggests that the patterning of topographic maps may be independent of whether axons branch or turn towards desired termination zones. Indeed, although our model fits more into the category of a 'growth cone guidance' model rather than a 'biased interstitial branching' model, it would be surprising if topographic mapping in different model systems was actually this distinct, given that axon targeting mechanisms are highly conserved between species. It is possible that instead there are general mechanisms that control map formation in most model systems, and that observed differences are due to physical constraints (e.g., gradient steepness, midbrain size, and axon number) and perhaps slight differences in the relative importance of mechanisms between species. Both guidance

and branching mechanisms may be specific realizations of a general axon guidance model, and both biased branching and growth cone guidance can perhaps be considered as limiting cases of this general model. We also suggest that this approach has advantages over explicitly modeling biased branching (e.g., Yates et al. (2004); Godfrey et al. (2009)), which requires many additional assumptions, and is dependent on a larger number of parameters than our model.

4.4 Model predictions

Our model makes a number of novel predictions. It has previously been suggested that the shapes of axon trajectories observed during normal development arise from differences in the strength of chemoaffinity along the two tectal axes (Gierer 1987). In contrast, our model predicts that these trajectories are influenced more strongly during initial ingrowth by the competitive influence of other fibers, with the influence of chemoaffinity based guidance becoming predominant only later (Fig. 2). A corollary of this is the prediction average trajectory shape should vary as the density of fibers arriving on the tectum/SC varies, which may be expected at different developmental timepoints in map formation. Similarly, the model predicts that all trajectories should be straighter if axon density is artificially reduced, for instance, when only single RGCs are present (Gosse et al. 2008). We also predict that, due to reduced competition, reduced axon density would cause a failure of the normally observed map expansion and compression when part of the retina or tectum is removed. This could be tested experimentally by a novel combination of single axon topography methods in zebrafish (Gosse et al. 2008) with surgical manipulation methods previously well established in other fish and frog species (see Udin and Fawcett (1988) or Goodhill and Xu (2005) for reviews of these types of experiments).

Our model also suggests a possible extension of the relative signaling hypothesis in terms of effector mechanisms. We propose that (1) a means by which the EphA receptor comparison is carried out could be through interaction with ephrinA ligands, (2) the molecular mechanism may be a thresholded mass action interaction between these receptor–ligand pairs, and (3) that this interaction causes repulsion primarily through forward signaling (i.e., the growth cone bearing the higher EphA level is repelled; see Methods for more detail). In our model, forward signaling through EphA receptors gives the best map collapse results (Supplementary Fig. 6). However, this is not at odds with work showing that reverse signaling (through ephrinA ligands) is involved in topographic mapping in other ways (for example, through the interaction between RGC ephrinA and EphA in the midbrain target, as in Rashid et al. (2005)). That is, this proposed predominance of forward signaling is specific to axon–axon interactions. This conclusion also offers an explanation for previous experiments demonstrating that temporal RGC axons are repelled by nasal axons, but that the reverse is not true (Bonhoeffer and Huf 1985). This result falls naturally out of an assumption that forward signaling through EphA is the dominant pathway in thresholded RGC axon interactions. Hence, we further predict that physically blocking the EphA–ephrinA interaction between two RGC axons, while maintaining guidance by tectal/SC molecular cues, would eliminate the map collapse phenomenon, and perhaps also the previously observed differences in repulsion between nasal and temporal RGC axons.

We also predict that EphA and ephrinA might exist in shapes that are at least approximately multiplicative mathematical inverses. For example, in the case of an EphA gradient of e^x, we would expect an ephrinA gradient of e^{-x}. The wild-type EphA gradient described by Reber et al. (2004), which we have used in this study, $R(x) = 0.26e^{2.3x} + 1.05$, has an approximately linear multiplicative inverse. Although this linear gradient is roughly consistent with previous experimental work, detailed quantitative measurements of both EphA and ephrinA protein gradients have not yet been performed, and hence this prediction remains to be tested.

Axon–axon interactions, like competition, can be enacted through neural activity or through molecular/physical means. Hence if map collapse is an axon–axon interaction-based phenomenon, it could be due to correlated activity, or molecular mechanisms, or both. Our model suggests that activity-independent axon–axon interactions are sufficient to induce this type of phenomenon, and that map collapse could therefore be stable under conditions of altered or absent correlated activity.

We also suggest an alternative explanation for the coarseness associated with activity-independent map formation, in that it may not be caused by physical limits associated with gradient sensing, but rather by noise contributions from multiple redundant mechanisms of map formation. Multiple mechanisms acting in concert give the mapping more flexibility to respond to different perturbations, but come at the expense of reduced precision in the final map. In contrast, activity-dependent mechanisms may have greater precision, but less flexibility, and rely on activity-independent mechanisms to give an overall structure to the map. In this way activity-dependent and activity-independent mechanisms work together to give flexibility and precision. More specifically, we predict that activity-independent map noise should vary predictably and consistently across the tectum/SC and be greater in areas of the midbrain target where receptor levels are higher (generally rostrally, e.g., Figs. 3, 4). We suggest that this is the result of more frequent subthreshold axon–axon interactions in these areas.

4.5 Conclusions

Together the results we present argue that the graded interaction of multiple constraints may be an important principle underlying retinotectal/retinocollicular map formation across a wide variety of circumstances, and that the computational form of this interaction need only be a simple linear sum. We have shown that a combination of chemoaffinity, competition, and axon–axon interactions can account for a wide range of experimental results. In addition, we suggest that forward signaling through EphA receptors in repulsive axon–axon interactions may be important in map collapse phenotypes, and in topographic map formation more generally. We suggest that in addition to further experimental work, this kind of simple but unified modeling has the potential to drive our understanding of neural map development forward.

Acknowledgments This study was funded by Australian Research Council grant DP0878939. We thank Massimo Hilliard, Duncan Mortimer, Michael Piper, and Rowan Tweedale for helpful discussions and comments on earlier versions of the manuscript.

References

Bastmeyer M, Ott H, Leppert CA, Stuermer CA (1995) Fish e587 glycoprotein, a member of the l1 family of cell adhesion molecules, participates in axonal fasciculation and the age-related order of ganglion cell axons in the goldfish retina. J Cell Biol 130(4):969–976

Bonhoeffer F, Huf J (1985) Position-dependent properties of retinal axons and their growth cones. Nature 315(6018):409–410

Brown A, Yates PA, Burrola P, no DO, Vaidya A, Jessell TM, Pfaff SL, O'Leary DD, Lemke G (2000) Topographic mapping from the retina to the midbrain is controlled by relative but not absolute levels of EphA receptor signaling. Cell 102(1):77–88

Caras IW (1997) A link between axon guidance and axon fasciculation suggested by studies of the tyrosine kinase receptor EphA5/REK7 and its ligand ephrin-A5/AL-1. Cell Tissue Res 290(2):261–264

Cheng HJ, Nakamoto M, Bergemann AD, Flanagan JG (1995) Complementary gradients in expression and binding of ELF-1 and Mek4 in development of the topographic retinotectal projection map. Cell 82(3):371–381

Cowan J, Friedman A (1991) Studies of a model for the development and regeneration of eye brain maps. In: Touretzky DS (ed) Advances in neural information processing systems III. Morgan Kaufman, San Mateo pp 3–10

Debski EA, Cline HT (2002) Activity-dependent mapping in the retinotectal projection. Curr Opin Neurobiol 12(1):93–99

Drescher U, Kremoser C, Handwerker C, Lschinger J, Noda M, Bonhoeffer F (1995) In vitro guidance of retinal ganglion cell axons by RAGS, a 25 kDa tectal protein related to ligands for Eph receptor tyrosine kinases. Cell 82(3):359–370

Feldheim DA, Kim YI, Bergemann AD, Frisén J, Barbacid M, Flanagan JG (2000) Genetic analysis of ephrin-A2 and ephrin-A5 shows their requirement in multiple aspects of retinocollicular mapping. Neuron 25(3):563–574

Fraser SE, Perkel DH (1990) Competitive and positional cues in the patterning of nerve connections. J Neurobiol 21(1):51–72. doi:10.1002/neu.480210105

Fujisawa H (1981) Retinotopic analysis of fiber pathways in the regenerating retinotectal system of the adult newt cynops pyrrhogaster. Brain Res 206(1):27–37

Gaze RM, Grant P (1978) The diencephalic course of regenerating retinotectal fibres in xenopus tadpoles. J Embryol Exp Morphol 44:201–216

Gaze RM, Keating MJ (1972) The visual system and "neuronal specificity". Nature 237(5355):375–378

Gierer A (1987) Directional cues for growing axons forming the retinotectal projection. Development 101(3):479–489

Gierer A (1983) Model for the retino-tectal projection. Proc R Soc Lond B Biol Sci 218(1210):77–93

Godfrey KB, Eglen SJ, Swindale NV (2009) A multi-component model of the developing retinocollicular pathway incorporating axonal and synaptic growth. PLoS Comput Biol 5(12):e1000600. doi:10.1371/journal.pcbi.1000600

Goodhill GJ, Richards LJ (1999) Retinotectal maps: molecules, models and misplaced data. Trends Neurosci 22(12):529–534

Goodhill GJ, Xu J (2005) The development of retinotectal maps: a review of models based on molecular gradients. Network 16(1):5–34

Gosse NJ, Nevin LM, Baier H (2008) Retinotopic order in the absence of axon competition. Nature 452(7189):892–895. doi:10.1038/nature06816

Hansen MJ, Dallal DJ, Flanagan JG (2004) Retinal axon response to ephrin-As shows a graded, concentration-dependent transition from growth promotion to inhibition. Neuron 42(5):717–730. doi:10.1016/j.neuron.2004.05.009

Harris WA, Holt CE, Bonhoeffer F (1987) Retinal axons with and without their somata, growing to and arborizing in the tectum of xenopus embryos: a time-lapse video study of single fibres in vivo. Development 101(1):123–133

Harris WA (1982) The transplantation of eyes to genetically eyeless salamanders: visual projections and somatosensory interactions. J Neurosci 2(3):339–353

Hayes WP, Meyer RL (1988) Normal and regenerating optic fibers in goldfish tectum: HRP-EM evidence for rapid synaptogenesis and optic fiber-fiber affinity. J Comp Neurol 274(4):516–538. doi:10.1002/cne.902740404

Honda H (2003) Competition between retinal ganglion axons for targets under the servomechanism model explains abnormal retinocollicular projection of Eph receptor-overexpressing or ephrin-lacking mice. J Neurosci 23(32):10,368–10,377

Honda H (1998) Topographic mapping in the retinotectal projection by means of complementary ligand and receptor gradients: a computer simulation study. J Theor Biol 192(2):235–246. doi:10.1006/jtbi.1998.0662

Hope RA, Hammond BJ, Gaze RM (1976) The arrow model: retinotectal specificity and map formation in the goldfish visual system. Proc R Soc Lond B Biol Sci 194(1117):447–466

Horder TJ (1971) Retention, by fish optic nerve fibres regenerating to new terminal sites in the tectum, of 'chemospecific' affinity for their original sites. J Physiol 216(2):53P–55P

Kaas JH (1997) Topographic maps are fundamental to sensory processing. Brain Res Bull 44(2):107–112

Kaethner RJ, Stuermer CA (1992) Dynamics of terminal arbor formation and target approach of retinotectal axons in living zebrafish embryos: a time-lapse study of single axons. J Neurosci 12(8):3257–3271

Koulakov AA, Tsigankov DN (2004) A stochastic model for retinocollicular map development. BMC Neurosci 5:30. doi:10.1186/1471-2202-5-30

McLaughlin T, O'Leary DDM (2005) Molecular gradients and development of retinotopic maps. Annu Rev Neurosci 28:327–355. doi:10.1146/annurev.neuro.28.061604.135714

Nakamoto M, Cheng HJ, Friedman GC, McLaughlin T, Hansen MJ, Yoon CH, O'Leary DD, Flanagan JG (1996) Topographically specific effects of ELF-1 on retinal axon guidance in vitro and retinal axon mapping in vivo. Cell 86(5):755–766

Overton KJ, Arbib MA (1982a) Systems matching and topographic maps: the branch-arrow model (BAM). In: Amari S, Arbib MA (eds) Competition and cooperation in neural nets. Lecture Notes in Biomathematics. Springer, Berlin, Heidelberg, New York. A5:202–225

Overton KJ, Arbib MA (1982b) The extended branch-arrow model of the formation of retino-tectal connections. Biol Cybern 45(3):157–175

Pasquale EB (2005) Eph receptor signalling casts a wide net on cell behaviour. Nat Rev Mol Cell Biol 6(6):462–475. doi:10.1038/nrm1662

Pittman AJ, Law MY, Chien CB (2008) Pathfinding in a large vertebrate axon tract: isotypic interactions guide retinotectal axons at multiple choice points. Development 135(17):2865–2871. doi:10.1242/dev.025049

Prestige MC, Willshaw DJ (1975) On a role for competition in the formation of patterned neural connexions. Proc R Soc Lond B Biol Sci 190(1098):77–98

Rashid T, Upton AL, Blentic A, Ciossek T, Knöll B, Thompson ID, Drescher U (2005) Opposing gradients of ephrin-As and EphA7 in the superior colliculus are essential for topographic mapping in the mammalian visual system. Neuron 47(1):57–69. doi:10.1016/j.neuron.2005.05.030

Reber M, Burrola P, Lemke G (2004) A relative signalling model for the formation of a topographic neural map. Nature 431(7010):847–853. doi:10.1038/nature02957

Ruthazer ES, Cline HT (2004) Insights into activity-dependent map formation from the retinotectal system: a middle-of-the-brain perspective. J Neurobiol 59(1):134–146. doi:10.1002/neu.10344

Schmidt JT, Cicerone CM, Easter SS (1978) Expansion of the half retinal projection to the tectum in goldfish: an electrophysiological and anatomical study. J Comp Neurol 177(2):257–277. doi:10.1002/cne.901770206

Scicolone G, Ortalli AL, Carri NG (2009) Key roles of Ephs and ephrins in retinotectal topographic map formation. Brain Res Bull 79(5):227–247. doi:10.1016/j.brainresbull.2009.03.008

Simon DK, O'Leary DD (1992) Development of topographic order in the mammalian retinocollicular projection. J Neurosci 12(4):1212–1232

Simpson HD, Mortimer D, Goodhill GJ (2009) Theoretical models of neural circuit development. Curr Top Dev Biol 87:1–51

Sperry R (1963) Chemoaffinity in the orderly growth of nerve fiber patterns and connections. Proc Natl Acad Sci USA 50:703–710

Straznicky K, Gaze RM (1971) The growth of the retina in Xenopus laevis: an autoradiographic study. J Embryol Exp Morphol 26(1):67–79

Stuermer CA, Raymond PA (1989) Developing retinotectal projection in larval goldfish. J Comp Neurol 281(4):630–640. doi:10.1002/cne.902810411

Stuermer CA (1988) Trajectories of regenerating retinal axons in the goldfish tectum: II. Exploratory branches and growth cones on axons at early regeneration stages. J Comp Neurol 267(1):69–91. doi:10.1002/cne.902670106

Thivierge JP, Marcus GF (2007) The topographic brain: from neural connectivity to cognition. Trends Neurosci 30(6):251–259. doi:10.1016/j.tins.2007.04.004

Tsigankov DN, Koulakov AA (2006) A unifying model for activity-dependent and activity-independent mechanisms predicts complete structure of topographic maps in ephrin-A deficient mice. J Comput Neurosci 21(1):101–114. doi:10.1007/s10827-006-9575-7

Udin SB, Fawcett JW (1988) Formation of topographic maps. Annu Rev Neurosci 11:289–327. doi:10.1146/annurev.ne.11.030188.001445

Weber C, Ritter H, Cowan J, Klaus Obermayer K (1997) Development and regeneration of the retinotectal map in goldfish: a computational study. Philos Trans Biol Sci 352(1361):1603–1623

Whitelaw VA, Cowan JD (1981) Specificity and plasticity of retinotectal connections: a computational model. J Neurosci 1(12):1369–1387

Wilkinson DG (2001) Multiple roles of Eph receptors and ephrins in neural development. Nat Rev Neurosci 2(3):155–164

Willshaw D (2006) Analysis of mouse EphA knockins and knockouts suggests that retinal axons programme target cells to form ordered retinotopic maps. Development 133(14):2705–2717. doi:10.1242/dev.02430

Willshaw DJ, Price DJ (2003) Models for topographic map formation. In: van Ooyen A (ed) Modeling Neural Development. MIT Press, Cambridge, MA. pp 213–244

Willshaw DJ, von der Malsburg C (1979) A marker induction mechanism for the establishment of ordered neural mappings: its application to the retinotectal problem. Philos Trans R Soc Lond B Biol Sci 287(1021):203–243

Yates PA, Holub AD, McLaughlin T, Sejnowski TJ, O'Leary DDM (2004) Computational modeling of retinotopic map development to define contributions of EphA-ephrinA gradients, axon–axon interactions, and patterned activity. J Neurobiol 59(1):95–113. doi:10.1002/neu.10341

Yoon MG (1976) Progress of topographic regulation of the visual projection in the halved optic tectum of adult goldfish. J Physiol 257(3):621–643

Yoon MG (1973) Retention of the original topographic polarity by the 180 degrees rotated tectal reimplant in young adult goldfish. J Physiol 233(3):575–588